Everyone works better together: rational improvements to radio- and immunotherapy combinations

Frijlink, E.S.

2

PD-1 and CTLA-4 blockade promote CD86-driven Treg responses upon radiotherapy of lymphocyte-depleted cancer

Manuscript in revision – J. Clin. Invest.

Elselien Frijlink[1,2], Douwe M.T. Bosma[2], Thomas W. Battaglia[3], Julia Busselaar[2], Mo D. Staal[2], Inge Verbrugge[1,4] and Jannie Borst[2]

[1]Division of Tumor Biology and Immunology and Oncode Institute, The Netherlands Cancer Institute, Amsterdam, The Netherlands
[2]Department of Immunology and Oncode Institute, Leiden University Medical Center, Leiden, The Netherlands
[3]Division of Molecular Oncology and Immunology and Oncode Institute, The Netherlands Cancer Institute, Amsterdam, The Netherlands
[4]Present address: Genmab, Utrecht, The Netherlands.

Abstract

Radiotherapy (RT) is considered immunogenic, but clinical data demonstrating RT-induced T-cell priming are scarce. Here, we show in a mouse tumor model representative of human lymphocyte-depleted cancer that RT enhances spontaneous priming of regulatory T-cells (Treg) by the tumor. These Tregs impede RT-induced $CD8^+$ cytotoxic T-cell (CTL)-mediated tumor control. CTLA-4 or PD-1 blockade, which enables CD28 costimulation, further increased RT-induced Treg responses and failed to improve tumor control. We discovered that upon RT, CD28-ligands CD86 and CD80 differentially affected the Treg response. Only CD86 blockade promoted the $PD\text{-}L1^+CD80^+$ costimulatory status of conventional (c)DCs and prevented the Treg response. Blockade of CD86 alone or in combination with PD-1 enhanced intra-tumoral CTL accumulation and significantly increased RT-induced tumor regression and overall survival. We advise that combining RT with PD-1 and/or CTLA-4 blockade may be counterproductive in tumors that are Treg dominant. However, combining RT with CD86 blockade can promote control of such tumors by enabling a CTL response.

Summary

In lymphocyte-depleted cancer, PD-1 and CTLA-4 blockade promote radiotherapy-induced Treg responses in a CD86-dependent manner and prevent $CD8^+$ T-cell mediated tumor control.

Introduction

Immunotherapies, particularly antibody-based immune-checkpoint blockade (ICB), are now a mainstay in managing multiple cancer types. However, only a minority of patients shows durable clinical responses[1], which is partially attributed to the immune composition of the tumor[2]. Pan-cancer transcriptome analyses have subdivided human cancer types into different classes, based on the intra-tumoral immune cell composition and cell states[3,4]. These analyses identified that ICB responsiveness only occurs in tumors that are infiltrated by effector-type $CD4^+$ and $CD8^+$ T cells[4]. To achieve clinical benefit in poorly immunogenic cancers devoid of effector T-cells, anti-tumor immune interventions therefore should elicit *de novo* T-cell responses[5]. In attempts to accomplish this, ICB is combined with RT in multiple clinical trials[6]. The combination of ICB with RT is attractive for multiple reasons: 1) RT-induced tumor cell death causes tumor debulking, which may alleviate systemic immune suppression, 2) RT can modulate the tumor micro-environment (TME) and render it more permissive for T cell-mediated tumor destruction[7], and 3) RT can support systemic anti-tumor immunity by generating new tumor-specific T-cell responses in the tumor-draining lymph nodes (TdLNs), in a process called T-cell priming.

The capacity of RT to induce *de novo*, systemic anti-tumor T-cell responses has been much advertised, based on theoretical grounds[8] and on observations in mouse models[9-11]. Upon RT-induced tumor cell destruction, cell debris will be released that contains tumor-derived antigens and danger-associated molecular patterns (DAMPs)[12,13]. This debris is engulfed locally by migratory, conventional dendritic cells (cDCs) that are activated by DAMPs and subsequently migrate to TdLNs and initiate T-cell responses. To prime $CD8^+$ T cells, the cDC1 subset is required that excels in cross-presenting peptides from phagocytosed proteins in MHC class I (MHC-I) molecules. Moreover, activated cDC1s give $CD8^+$ T cells the instruction to differentiate into competent CTLs via specific costimulatory and cytokine signals[14]. The potential of RT to induce T-cell priming and consequent systemic immunity predicts that it may potentiate abscopal effects, i.e. tumor regression outside the field of radiation. Clinically, such observations are extremely rare[15], indicating that there are impediments in this process[7]. In specific mouse tumor models, RT has repeatedly shown to induce T-cell infiltration not only of the irradiated tumor, but also of a tumor implanted on a non-irradiated site in the same mouse[16-18]. However, this observation is primarily restricted to tumors that contain dominant, non-self antigens.

Currently approved ICB immunotherapies, i.e. CTLA-4 and PD-(L)1 blockade, both promote T-cell costimulation by cDCs. PD-1 is a co-inhibitory receptor that attenuates T-cell responses by extinguishing downstream signaling of CD28[19]. CD28 costimulatory signals amplify and add to T-cell receptor (TCR)/CD3 signals to support division, metabolism, and survival of newly activated $CD4^+$ and $CD8^+$ T-cells[20]. When PD-1 binds either of its ligands PD-L1 or PD-L2, its cytoplasmic tail

recruits the SHP2 tyrosine phosphatase. This enzyme can then dephosphorylate the cytoplasmic tail of activated CD28, thus abrogating its downstream signaling[19]. The co-inhibitory receptor CTLA-4 is constitutively expressed on Tregs[21,22] and downregulates the CD28 ligands CD80 and CD86 on cDCs. Therefore, CTLA-4 attenuates the ability of cDCs to induce CD28 costimulation of conventional, non-regulatory T cells (Tconvs)[23]. Thus, CTLA-4 and PD-1 use different mechanisms, but both control T-cell responses by suppressing CD28 costimulation.

Thus far, clinical effects of combining RT with CTLA-4 or PD-1 targeting ICB are disappointing[6,24-27]. For example, RT as induction treatment did not enhance PD-1 blockade efficacy in metastatic triple negative breast cancer (TNBC) patients, nor did it improve T-cell infiltration in the TME[24]. Therefore, we must better understand the molecular mechanisms underlying RT-induced T-cell responses. In mouse models, tumors that are spontaneously immunogenic and become infiltrated with tumor-specific effector T cells during their development, have been shown to regress upon RT alone[28], or in combination with ICB[29], without a requirement for *de novo* T-cell priming. In such T-cell infiltrated tumors, the T cells already present in the TME can apparently exert their effector functions locally upon RT. However, in tumors that lack pre-existing tumor-specific effector T-cells, RT will have to induce new T-cell priming to allow for T-cell mediated tumor control. This may be hampered by lack of antigens and/or DAMPs released by the tumor[30,31] and/or by tumor-imposed immunosuppression[32]. We therefore examined in the current study how the T-cell response to RT proceeds in a mouse tumor model representing human lymphocyte-depleted cancer types. We found that Treg priming induced by RT prevented CTL-mediated tumor control. Importantly, CTLA-4 or PD-1 blockade further increased this Treg response. We discovered that selective inhibition of CD86 either alone or in combination with PD-1 blockade prevented the RT-induced Treg response, and enabled CTL priming and tumor control. We advise that combining RT with PD-(L)1 and/or CTLA-4-targeting ICB can be counterproductive in lymphocyte-depleted cancers and identify CD86 as an alternative target for ICB in such cases.

Results

RT response is deficient in T-cell depleted human tumor types

To identify how the tumor immune cell composition influences RT responses in human cancer, we examined the relationship between immune phenotype and RT efficacy in a wide variety of cancers. Using records from The Cancer Genome Atlas (TCGA), we identified five previously characterized pan-cancer immune phenotypes[3] in patients for which RT treatment was specified (Figure **S1A,B**). These immune phenotypes are described as "wound healing" (C1), "IFNγ dominant" (C2), "inflammatory" (C3), "lymphocyte depleted" (C4) and "immunologically quiet" (C5). While RT had a positive effect on overall survival (OS) in tumors classified as C1-3 immune subtypes, RT had a negative effect on OS in the C4 and C5 subtypes (Figure **1A**) that are identified by low lymphocyte- and high myeloid cell content[3]. The remarkably defective response to RT of tumors with a C4 and C5 immune phenotype prompted us to examine the underlying mechanism.

To perform mechanistic studies, we set out to find a mouse tumor model with a C4/C5-like lymphocyte depleted phenotype. We trained a K-nearest neighbor (KNN) classifier to distinguish between the C3 versus C4/C5 immune subtypes (Figure **S1C**) and subsequently applied our model to microarray data of murine (C57BL/6)-derived MC38 and TC-1 tumor models[33]. We found similarity between the colon carcinoma cell line MC38 and the C3 subtype and between the lung carcinoma cell line TC-1 and the C4/5 subtype (Figure **1B**). Despite the presence of neo-antigens and virus-related antigens respectively[34,35], the MC38 tumor is immunogenic and raises a high T-cell infiltrate[18], whereas the TC-1 tumor does not[36]. In concert with this, MC38 is responsive to ICB[37], whereas TC-1 is not[38]. Accordingly, flow cytometry analysis revealed a significantly lower proportion of $CD8^+$ T cells in TC-1 tumors as compared to MC38 tumors (Figure **1C**).

We assessed how MC38 and TC-1 tumors respond to RT, using three consecutive doses of 8 Gy (3x 8 Gy) or a single dose of 20 Gy, regimens that are described as immune stimulatory in mouse tumor models[9,39]. Both regimens led to MC38 tumor control, but were much less effective in TC-1 tumor control (Figure **1D**). This agrees with the finding that the pre-existing T-cell infiltrate in the MC38 tumor contributes to the RT response[28] and suggests impediments for immune-mediated control of the TC-1 tumor upon RT. We therefore continued our study with the TC-1 tumor to examine the RT-induced T-cell response in this representative of lymphocyte depleted cancer.

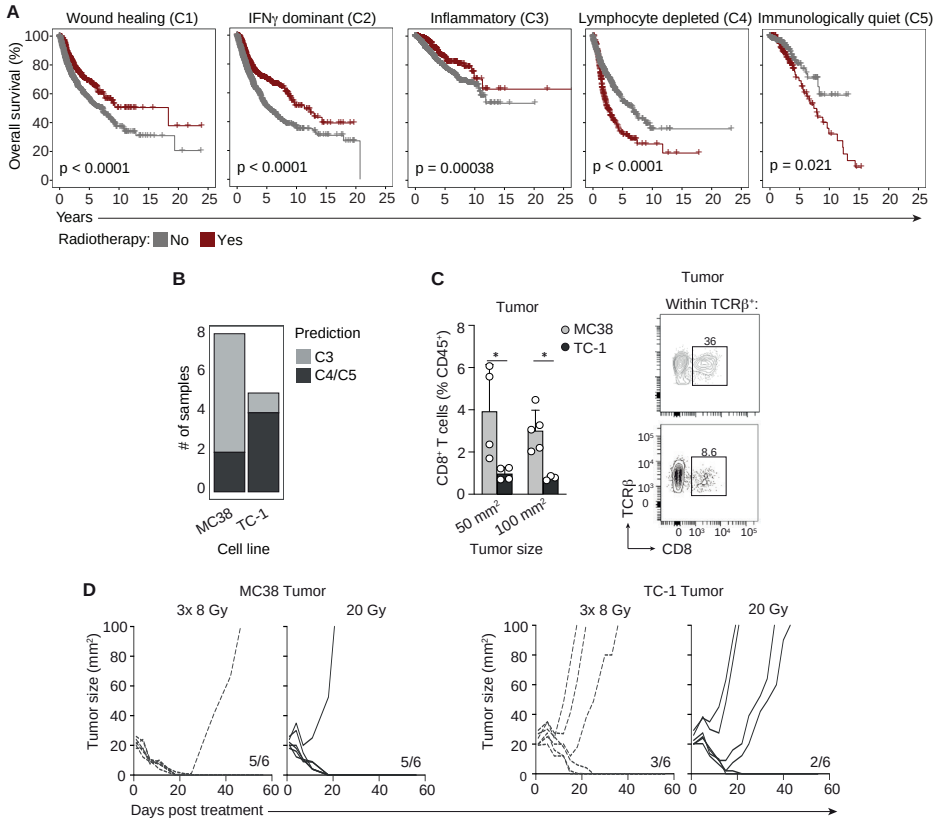

Figure 1. Lymphocyte depleted (C4/5) human cancers have suboptimal response to RT and are modelled by the murine TC-1 tumor.

(**A**) Kaplan-Meier OS curves obtained from TCGA for patients receiving RT (red) or not (grey) within the C1 "wound healing" (n=2136), C2 "IFNγ dominant" (n=2296), C3 "inflammatory" (n=1903), C4 "lymphocyte depleted" (n=1055) and C5 "Immunologically quiet" (n=354) cancer immune subtypes. Log-rank p-values were generated using a Cox proportional-hazards model. (**B**) C3 "inflammatory" versus C4/C5 "lymphocyte depleted" model predictions from transcriptome data of C57BL/6- syngeneic MC38 and TC-1 transplantable tumors. (**C**) Frequency of $CD8^+$ T cells among $CD45^+$ cells in MC38 (total n=9) and TC-1 (total n=7) tumors measured at the indicated tumor sizes (left), and representative flow cytometry plots (right) depicting the percentage of $CD8^+$ T cells within $TCR\beta^+$ cells in 50 mm^2 MC38 (grey) and TC-1 (black) tumors. (**D**) Tumor growth curves of MC38 (n=6/group, left) and TC-1 (n=6/group, right) tumor-bearing mice treated with either 8 Gy over 3 days (3x 8 Gy) or a single dose of 20 Gy RT. Ratios indicate the number of mice out total treated that showed full recovery upon RT. Error bars indicate SD. *P < 0.05, Mann-Whitney test.

Despite high myeloid and Treg content, the RT response of TC-1 is CD8$^+$ T-cell dependent

In the TME of the TC-1 tumor, the T-cell compartment, consisting of CD8$^+$ and CD4$^+$ Tconvs and FOXP3$^+$ Tregs, comprised only 11.1% of the CD45$^+$ hematopoietic cell infiltrate, as identified by flow cytometry. Conversely, myeloid cells comprised 62.5% of the CD45$^+$ cell infiltrate, including macrophages and neutrophils (Figure **2A,** Figure **S1D**). Tumors often raise systemic immune responses that may contribute to immunosuppression[40]. We therefore examined the spontaneous immune response to the TC-1 tumor not only in the tumor, but also in the axillary tumor-draining lymph node (TdLN) and non-TdLN of the mice. LyC6$^+$ monocytes were enriched in the tumor, as well as in the TdLN, but not in the non-TdLN (as compared to the axillary LN in tumor-free mice) (Figure **2B**). We analyzed the CD3$^+$ lymphocytes in tumor and LNs in detail by spectral flow cytometry. FlowSOM-guided clustering analysis and Uniform Manifold Approximation and Projection (UMAP)-dimension reduction (Figure **S1E,F**) identified seven main clusters, including CD8$^+$ and CD4$^+$ (FOXP3$^-$) Tconvs, proliferating (Ki67$^+$) CD8$^+$ and CD4$^+$ T cells, central (c)Tregs, effector (e)Tregs and CD4$^-$/CD8$^-$ T cells. After development in the thymus, Tregs populate secondary lymphoid organs, where they stay as cTregs to prevent responses of autoreactive Tconvs. Alternatively, in response to antigen and inflammatory signals, cTregs can expand and differentiate into eTregs that migrate to peripheral tissues to suppress inflammation[21]. Consistent with these findings, the eTreg population was proliferating and had high expression of the effector marker ICOS, next to steady-state Treg markers FOXP3, CTLA-4 and CD25, whereas cTregs did not proliferate, had no ICOS expression and lower expression of the Treg markers (Figure **2C**, Figure **S1G**). Quantification of the identified populations revealed no increase in proliferating CD8$^+$ or CD4$^+$ Tconvs in LNs upon TC-1 tumor outgrowth (Figure **S1H**). However, compared to naïve mice, the frequency of eTregs – but not cTregs – in the TdLN was significantly increased in tumor-bearing mice and eTregs were also present in the tumor (Figure **2D**). Thus, during its outgrowth, the TC-1 tumor recruits Ly6C$^+$ monocytes to the TdLN and stimulates eTreg formation in the TdLN, and these cells also populate the tumor, highlighting the communication between the tumor and TdLN[40,41].

Importantly, RT with either 20 Gy or 3x 8 Gy significantly augmented CD8$^+$ T-cell infiltration of the TC-1 tumor, as measured in frequency (Figure **2E**, Figure **S2A**) and absolute cell number (Figure **2F**). These tumor-infiltrating CD8$^+$ T cells were functional CTLs, as evidenced by the expression of Granzyme B (GZB) and the effector cytokines IFNγ and TNFα (Figure **2G**). The intra-tumoral frequency of (FOXP3$^-$) CD4$^+$ Tconvs was not significantly altered by RT (Figure **S2A,B**). Systemic depletion of CD8$^+$ T cells, but not of CD4$^+$ T cells (Figure **S2C,D)**, significantly reduced RT-induced mouse survival (Figure **2H**), arguing that the RT-induced CTL response makes a major contribution to control of the TC-1 tumor by RT. This finding suggests that there might be a window of opportunity to improve RT-induced, CTL-mediated control of lymphocyte depleted cancers.

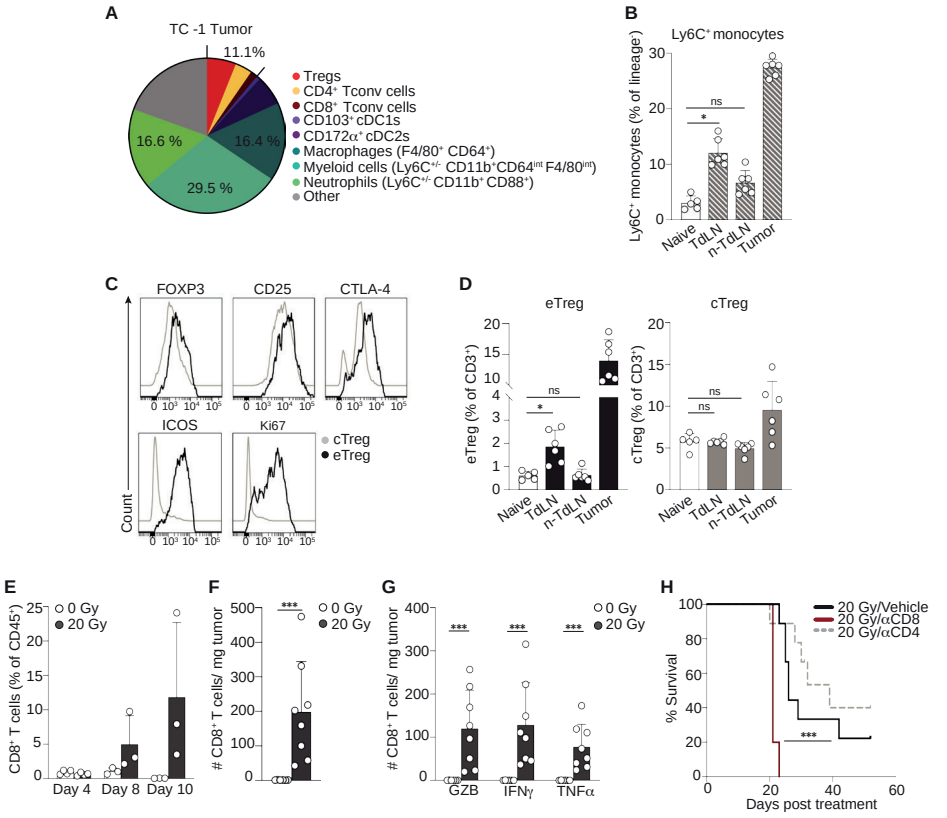

Figure 2. Treg- and myeloid cell-rich TC-1 tumor shows CD8⁺ T-cell dependent RT response.
(**A**) The frequency of the different indicated immune cell populations among CD45⁺ cells as determined by flow cytometry in 50 mm² TC-1 tumors (n=6). (**B-D**) Flow cytometric analysis of single cell suspensions from TdLN, non-TdLN and tumors of 100 mm² TC-1 tumor-bearing (n=6) and age-matched naïve mice (n=5). (**B**) Percentage of Ly6C⁺ monocytes among CD3⁻CD19⁻NK1.1⁻ (lineage⁻) cells found in the axillary LN of naïve mice and in indicated tissues of tumor-bearing mice. (**C**,**D**) cTregs and eTregs were defined as indicated in Figure **S1E-G**. FlowSOM guided clustering was performed on 5000 randomly selected cells per sample within the CD3⁺ lymphocyte population. (**C**) Representative histograms depicting expression of indicated markers on cTreg and eTreg populations in the right axillary LNs of naïve and TC-1 tumor bearing mice. (**D**) Percentage of eTregs (left) and cTregs (right) among CD3⁺ cells in the indicated tissues. (**E-H**) Monitoring by flow cytometry of the CD8⁺ T-cell response to 20 Gy RT (n=3-8) or control (0 Gy, n=3-6) in TC-1 tumors. (**E**) Frequency of CD8⁺ T cells among CD45⁺ T cells at the indicated time points post RT. (**F**) Absolute number (#) of total CD8⁺ T cells or (**G**) granzyme B (GZB), IFNγ, or TNFα-expressing CD8⁺ T cells per milligram (mg) tumor tissue at day 8 post RT. IFNγ and TNFα were measured after in vitro PMA/Ionomycin stimulation. (**H**) Overall survival of TC-1 tumor-bearing mice treated with 20 Gy RT at day 0 in combination with vehicle (PBS, n=9) or depleting mAbs specific for CD8 (n=5) or CD4 (n=9). ***P < 0.001 (Mantel-Cox analysis). Data are from one experiment representative of at least two experiments. Error bars indicate SD. *P < 0.05, *** P < 0.001, Kruskal-Wallis test with uncorrected Dunn's post hoc analysis in **B** and **D**, Mann-Whitney test in **F** and **G.** ns; no significance.

RT of the TC-1 tumor induces CTL priming, next to a Treg response that limits tumor control

The influx of effector CTLs in the irradiated TC-1 tumor likely originated from the induction of a *de novo* $CD8^+$ T-cell response in the TdLN, resulting from the release of tumor antigens and DAMPs by RT[12]. In highly antigenic mouse models, T-cell priming proved important for durable RT-induced anti-tumor immunity[9,10]. We wanted to examine whether this is also the case for poorly immunogenic, T-cell depleted tumors such as TC-1. To visualize new T-cell priming after RT, mice were treated with the S1P-receptor agonist FTY720, which traps T cells in LNs[42]. In this way, the window to identify newly primed T cells in the TdLN is enlarged. As done throughout this study, the tumor was selectively irradiated by imaged-guided RT and the mice were treated before and after RT with FTY720 or vehicle. FTY720 efficacy was confirmed by the elimination of circulating $CD8^+$ and $CD4^+$ T cells in peripheral blood (Figure **S3A**), and treatment with FTY720 did not affect tumor development (Figure **S3B**). At day 8 after RT, T-cell priming and effector differentiation were analyzed in the TdLN. In presence of FTY720, a significant RT-induced increase in GZB^+- and $IFN\gamma^+TNF\alpha^+$-double expressing $CD8^+$ T cells was revealed (Figure **3A,B**), while RT did not alter the frequency of effector phenotype $CD4^+$ T cells (Figure **S3C**). Moreover, FTY720 treatment revealed that a large part of the effector $CD8^+$ T cells present in the tumor after RT originated from the TdLN, since their frequency in the tumor was significantly reduced upon FTY720 treatment (Figure **3C,D**). The same was observed for effector $CD4^+$ T cells (Figure **S3D**). Thus, in the lymphocyte-depleted TC-1 tumor model, RT elicits priming of $CD8^+$ T cells that subsequently migrate into the irradiated tumor.

However, despite RT-induced CTL priming, not all TC-1 tumor-bearing mice were cured (Figure **1D**). Since the TC-1 tumor induced Treg priming during its development, and because of the described increase of Tregs in the TME upon RT[32,43,44], we considered that RT might enhance the Treg response in the TC-1 tumor setting. Several reports describe that Tregs require antigen-dependent activation and expansion in the TdLN prior to migration to the tumor[41,45]. We observed that Treg frequencies (Figure **3E,** Figure **S3E**) and absolute numbers (Figure **S3F**), were significantly increased in TdLN and tumor, but not in the non-TdLN, at day 8 after RT. In addition, Treg frequency was increased in blood over time (Figure **3F**) and the percentage of proliferating ($Ki67^+$) Tregs was enhanced in the TdLN but not in the non-TdLN following RT (Figure **3G,** Figure **S3G**). This coincided with a significant decrease in the frequency of proliferating Tregs in the TME (Figure **3G**, Figure **S3G**). These data clearly demonstrate RT-induced Treg priming in the TdLN, followed by migration of these cells into the irradiated TME, rather than RT-induced Treg expansion in the TME[43]. Thus, despite new $CD8^+$ T-cell responses, concomitant RT-induced Treg priming significantly lowered the $CD8^+$ T cell/Treg ratio in the TdLN, while maintaining the unfavorable $CD8^+$ T cell/Treg ratio in the tumor (Figure **3H**). This suggests that Tregs might be an impediment to CTL-mediated tumor control. To test this, we

treated mice with an Fc-modified antibody to CD25[46] that efficiently depleted peripheral and intra-tumoral Tregs (Figure **S4A,B**), but not CD8⁺ or CD4⁺ Tconvs (Figure **S4C**). This intervention greatly improved TC-1 tumor control and overall survival in mice after 20 Gy RT (Figure **3I**, Figure **S4D,E**). We observed similar effects when mice were treated with 3x 8 Gy (Figure **S4F,G**).

Taken together, these data indicate that in the TC-1 tumor model, Tregs limit RT-mediated tumor eradication, likely by inhibiting the RT-induced CTL response.

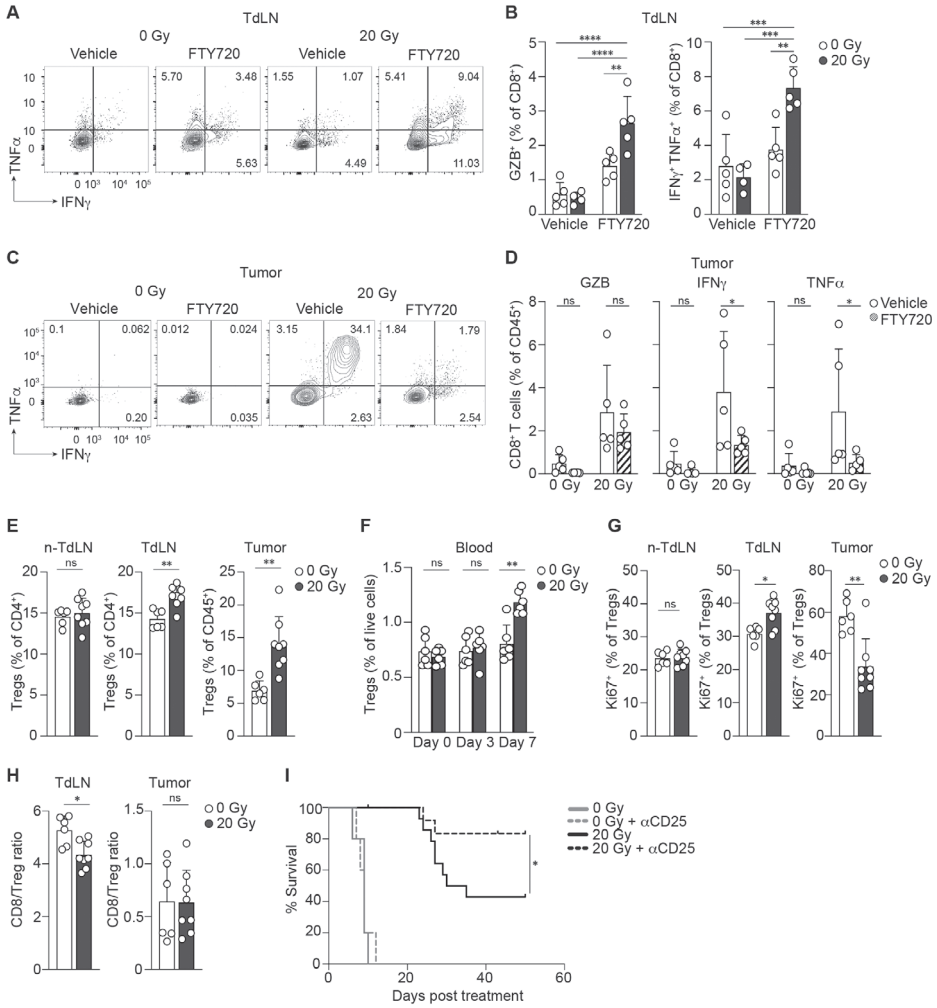

← Figure 3. RT of TC-1 induces concomitant priming of CTL- and Treg responses.
(**A-D**) Mice (n=4-5/group) were s.c injected with TC-1 tumor cells and the tumor was treated with 20 Gy RT when it reached ~20 mm^2 in size (day 0). Mice received FTY720 or vehicle (NaCl) by oral gavage, at days -1, 3 and 5. At day 8, TdLN (**A,B**) and tumor (**C,D**) were isolated and the $CD8^+$ T-cell response was analyzed by flow cytometry. (**A,C**) Representative flow cytometry plots depicting the percentage of $IFN\gamma^+$ and/or $TNF\alpha^+$ cells among $CD8^+$ T cells from the TdLN (**A**) and tumor (**C**). (**B,D**) Frequency of GZB^+, $IFN\gamma^+$ and/or $TNF\alpha^+$ cells among $CD8^+$ T cells from the TdLN (**B**) and tumor (**D**). IFNγ and TNFα were measured after in vitro PMA/Ionomycin stimulation for 3 h. (**E-H**) Monitoring of the ($FOXP3^+$ $CD25^+$) Treg response to 20 Gy RT (n=6-8) or control (0 Gy, n=6) in TC-1 tumor-bearing mice at day 8 post treatment. (**E**) Frequency of Tregs among $CD4^+$ T cells in the non-TdLN and TdLN, or among $CD45^+$ cells within the tumor. (**F**) In a separate experiment, the percentage of Tregs among live cells measured in blood at the indicated time points (n=6/group). (**G**) Percentage of $Ki67^+$ cells among Tregs in the indicated tissues. (**H**) The ratio of $CD8^+$ T cells to Treg cells in the TdLN and tumor post RT. Data in (G, H) is from the same experiment as in (E). (**I**) Overall survival of TC-1 tumor-bearing mice treated with 0 Gy (n=5) or 20 Gy RT (n=11-14/group) in combination with a depleting mAb against CD25 or vehicle (PBS) delivered I.P. at day -1 and 5 post RT. *P < 0.05 (Mantel-Cox analysis). Data are from one experiment representative of at least two experiments. Error bars indicate SD. *P < 0.05, **P < 0.01, *** P < 0.001, **** P < 0.0001, two-way Anova with Tukey's post hoc test in **A**, **C** and **F**, Mann-Whitney test in **E**, **G**, **H**. ns; no significance.

CTLA-4 blockade increases the RT-induced Treg response and does not improve tumor control

Blockade of CTLA-4 has been shown to enhance RT-induced tumor regression in mouse models[47,48] and clinical studies[25,26,49]. We next explored whether CTLA-4 inhibition could improve CTL-mediated TC-1 tumor control after RT in our lymphocyte-depleted TC-1 tumor setting. To study this, tumors were treated with RT when they reached 20 mm^2 as before (day 0) and a blocking antibody to CTLA-4, that does not deplete T-cells from tumor tissue[22,50], or vehicle was injected on day 0, 3, 6 and 9. Clearly, in the TC-1 tumor setting, anti-CTLA-4 treatment did not improve RT-induced tumor control or overall survival of the mice (Figure **4A,B**). Interestingly, CTLA-4 blockade increased the RT-induced Treg response in both TdLN and non-TdLN and the population of Tregs in the tumor remained high (Figure **4C**). To more comprehensively characterize how CTLA-4 blockade affected RT-induced T-cell responses, we performed FlowSOM-guided clustering analysis and dimensionality reduction on the $CD3^+$ populations in the different tissues (Figure **4D,E**). CTLA-4 blockade in context of RT significantly increased the frequencies of both eTregs and cTregs in the non-TdLN and TdLN, while the proportion of eTregs in the tumor did not change compared to RT alone (Figure **4F,G**). Importantly, we further observed that RT as a single treatment selectively increased the proportion of eTregs, but not of cTregs, in the TdLN and tumor (Figure **4G**), suggesting that RT is required to facilitate cTreg to eTreg conversion. Thus, the TC-1 tumor promotes eTreg priming, RT supports this process in addition to CTLA-4 blockade. Since Tregs are highly dependent on CD28 costimulation for their expansion[51-53], we propose that Tregs profit more from CTLA-4 blockade than Tconvs, due to their prevalence in the TdLN of the TC-1 tumor. Tregs may capitalize on the increased availability of CD80 and/or CD86 on cDCs following CTLA-4 blockade, resulting in augmented CD28 costimulation and subsequent Treg priming (Figure **4H**).

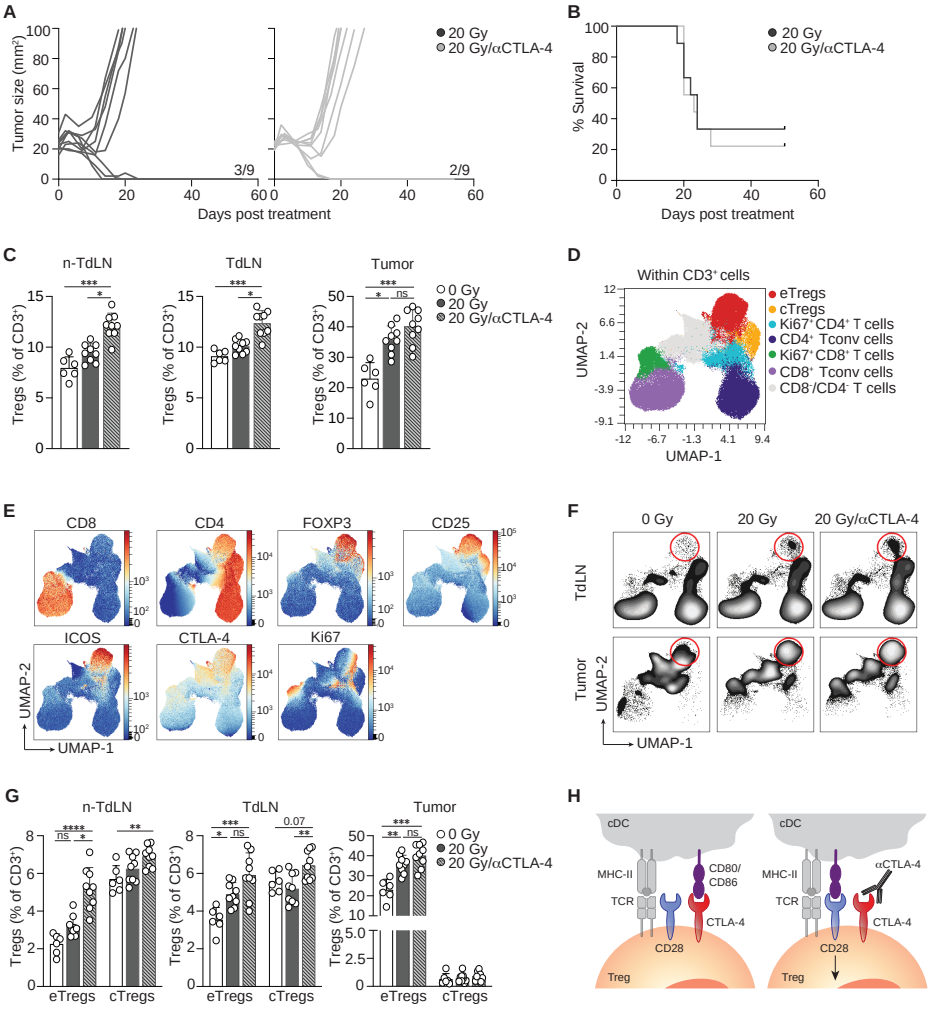

Figure 4. Blockade of CTLA-4 enhances RT-induced eTreg expansion.
Mice bearing TC-1 tumors received RT (20 Gy, n=9) or control treatment (0 Gy, n=6) when tumor size reached 20 mm² (day 0). Treatment with vehicle (PBS) or with a blocking mAb against CTLA-4 was given at day 0, 3, 6 and 9 and responses were monitored longitudinally (**A, B**) or by performing flow cytometric analysis of the non-TdLN, TdLN and tumor at day 8 post treatment (**C-G**). (**A**) Individual tumor growth curves and (**B**) overall survival of the mice in the indicated treatment groups. (**C**) Percentage of total Tregs among CD3⁺ lymphocytes in the indicated tissues at day 8. (**D-F**) UMAP display of 2500 randomly selected CD3⁺ cells per sample found in non-TdLN, TdLN and tumors at day 8 of all mice per treatment group. FlowSOM guided clustering (**D**) identifying the CD3⁺ cell populations (see also Figure **S1E)** and (**E**) representative heat map visualization of the markers that identify the CD3⁺ (T-cell) subpopulations. (**F**) UMAP visualization of the response of the CD3⁺ subpopulations in TdLN and tumor to the indicated treatments. The circles highlight the eTreg population. (**G**) Frequencies of eTregs and cTregs identified in (**D**) among CD3⁺ cells found in the indicated tissues at day 8 post treatment. (**H**) Graphic visualizing how Tregs could profit from CTLA-4 blockade. Data in this experiment are from one experiment representative of two experiments. Error bars indicate SD. *P < 0.05, **P < 0.01, *** P < 0.001, **** P < 0.0001, Kruskal-Wallis with Dunn's post hoc test. ns; no significance.

CD86 rather than CD80, promotes RT-induced Treg responses

The above findings highlight the importance of the CD28 costimulatory axis in regulating Treg expansion and raise the possibility that the CD28 ligands CD80 and/or CD86 may dictate Treg numbers after RT in the TC-1 tumor model. We therefore selectively blocked CD80 or CD86 in presence of RT and examined the T-cell response in detail by spectral flow cytometry as before, focusing on $CD3^+$ T-cell populations (Figure **5A,B**). Interestingly, blockade of CD86 significantly reduced the RT-induced eTreg population in non-TdLN, TdLN and tumor (Figure **5C,D**). After CD86 blockade, the frequency of eTregs in these tissues were comparable to those in non-irradiated mice (0 Gy). CD86 blockade also diminished the proportion of cTregs in the non-TdLN, suggesting a role for CD86 in the maintenance of steady-state cTregs. In contrast, CD80 blockade in the context of RT only reduced the frequency of eTregs in the TdLN (Figure **5C,D**). Thus, in the TC-1 tumor setting, CD86 is the selective CD28-ligand that supports the generation of an eTreg response after RT (Figure **5E**).

CD86 blockade in context of RT improves conventional (c)DC costimulatory status and CTL priming

To clarify how CD80/CD86 blockade may impact T-cell priming, we examined the trafficking and phenotype of migratory cDC1 and cDC2 that are responsible for this process[54-56]. cDC subsets were identified by flow cytometry as indicated in Figure **S5A**. The absolute number of cDC1s or cDC2 in the TdLN was not altered by RT alone as compared to control. However, cDC1 numbers were significantly increased when RT was combined with CD86 blockade, and there was a similar trend for cDC2s (Figure **6A**). CD86 is constitutively expressed on cDCs, while CD80 is upregulated upon activation[20]. In the context of RT, CD86 blockade significantly increased the expression of CD80, but not CD86 on both cDC1s and cDC2s (Figure **S5B,C**). CD86 and CD80 blockade did not significantly alter expression of CD40 or PD-L1 on either cDC1s or cDC2s (Figure **S5B,C**).

On the cDC membrane, CD80 can heterodimerize with PD-L1. This CD80:PD-L1 heterodimer can bind and engage CD28, but cannot bind to PD-1, nor can it be downregulated by CTLA-4[57,58]. It has been documented that co-expression of CD80 and PD-L1 on cDCs positively correlates with their CTL priming capacity against cancer, in agreement with increased formation of a CD28-costimulatory CD80:PD-L1 heterodimer[59]. We found in the TC-1 tumor model that upon RT, CD86 blockade significantly increased the frequency of cDC1s and cDC2s that co-expressed CD80 and PD-L1 (Figure **6B-D**). Furthermore, the frequency of $CD80^+$ $PD\text{-}L1^-$ cells was also increased, whereas the frequency of $CD80^-$ $PD\text{-}L1^+$ cells was decreased. Thus, in the TC-1 model, CD86 blockade in the context of RT likely favors CTL priming by increased presence of migratory cDC1s presenting tumor antigen in the TdLN and their improved costimulatory capacity.

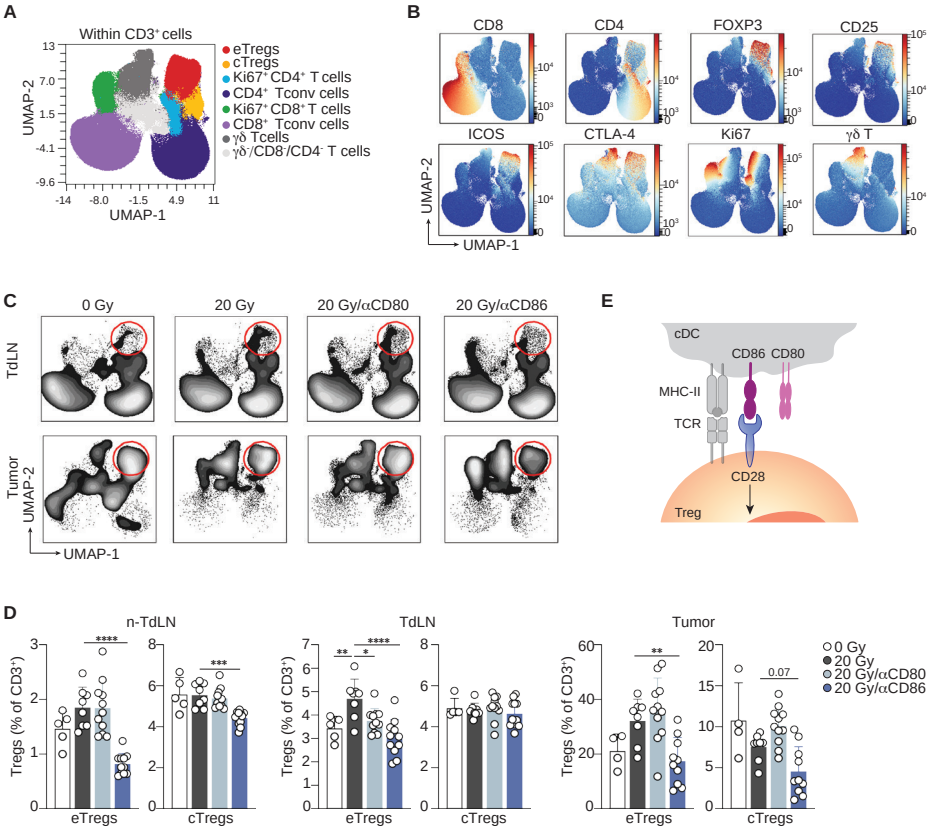

Figure 5. CD86, but not CD80, drives the RT-induced eTreg response.
Mice bearing 20 mm^2 TC-1 tumors received control treatment (0 Gy, n=5) or 20 Gy RT at day 0 in combination with either vehicle (PBS, n=8) or blocking mAb against CD80 (n=11) or CD86 (n=11) at day 0, 3 and 6. The CD3$^+$ lymphocyte response was monitored by flow cytometry in the non-TdLN, TdLN and tumor at day 8. (**A-C**) UMAP visualization of 2500 randomly selected CD3$^+$ cells per sample found in non-TdLN, TdLN and tumors at day 8 of all treatment groups combined. FlowSOM guided clustering (**A**) identifying the same populations as found in the previous figures and (**B**) representative heat maps of the markers included to determine the CD3$^+$ subpopulations. (**C**) Visualization of the response of the CD3$^+$ subpopulation in TdLN and tumor to the indicated treatments. The circles highlight the eTreg population. (**D**) Frequencies of eTregs and cTregs identified in (**B**) among CD3$^+$ cells found in the indicated tissues at day 8 post treatment. (**E**) Graphic visualization of how CD86, but not CD80, binds CD28 to support Treg expansion. Data are from one experiment representative of two experiments. Error bars indicate SD. *P < 0.05, **P < 0.01, *** P < 0.001, **** P < 0.0001, ordinary one-way Anova with Dunnett's post hoc test in **D**.

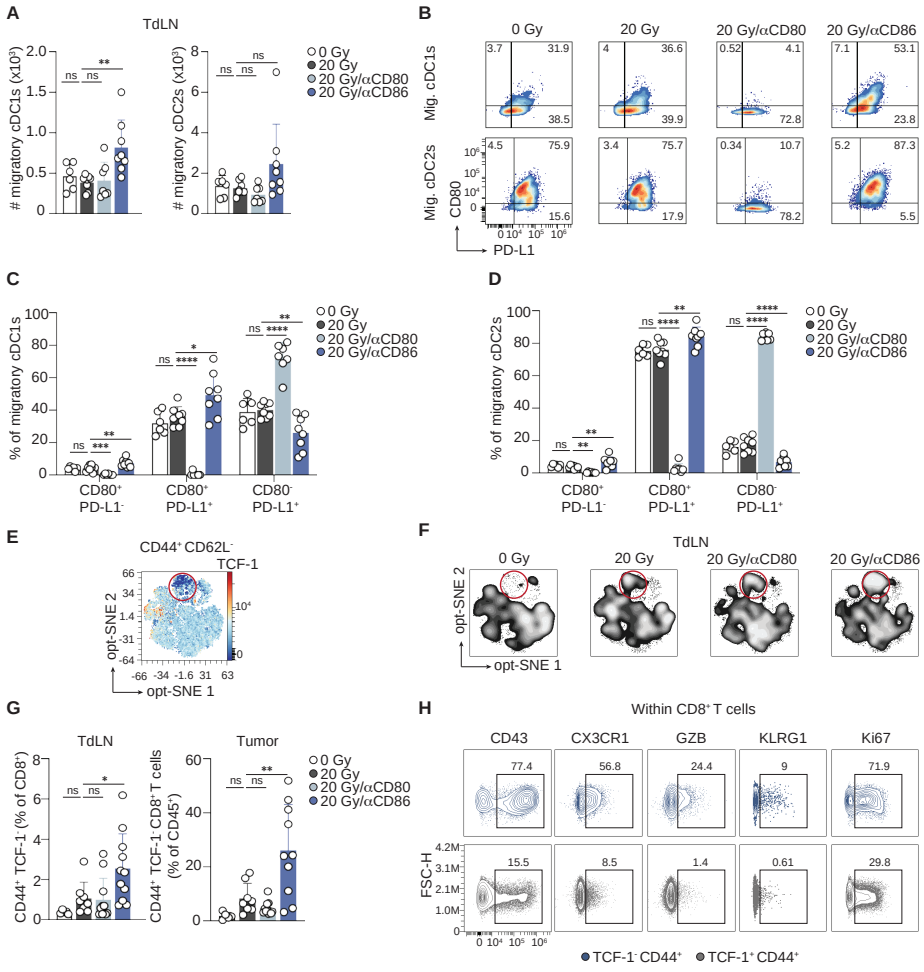

Figure 6. CD86 blockade in context of RT improves the conventional (c)DC costimulatory status and CTL priming.

(**A–D**) Mice bearing 20 mm² TC-1 tumors received 0 Gy (n=6) or 20 Gy RT at day 0 in combination with either vehicle (PBS, n=8) or blocking mAb against CD80 (n=7) or CD86 (n=8) at day 0, 3 and 6. The cDC response was monitored by flow cytometry in the TdLN at day 8. (**A**) Absolute counts (#) of migratory cDCs1 and cDC2s. (**B**) Representative concatenated (n=6-8) flow cytometry plots depicting the percentage of CD80⁺ and/or PD-L1⁺ cells among migratory cDC1s and cDC2s in the TdLN per treatment group. Numbers indicate percentages. (**C-D**) Quantification of the populations represented in (**B**) among migratory cDC1s (**C**) and migratory cDC2s (**D**) from the TdLN. (**E–H**) The CD8⁺ T cell response was monitored by flow cytometry in the same experiment described in Figure **5**. (**E,F**) Opt-SNE visualization of 1000 randomly selected CD44⁺ CD62L⁻ cells among CD8⁺ T cells per sample found in TdLNs at day 8 concatenated per treatment group. (**E**) Representative heat map of TCF-1 expression and (**F**) visualization of the TCF-1⁻ subpopulation in TdLN (encircled) in different treatment groups. (**G**) Frequency of CD44⁺ TCF-1⁻ cells among CD8⁺ T cells found in the TdLN and among CD45⁺ cells in the tumor at day 8 post treatment. (**H**) Concatenated (n=11) contour plots depicting expression of the indicated markers on CD44⁺ TCF-1⁻ cells and CD44⁺ TCF-1⁺ cells within CD8⁺ T cells in the TdLN. Numbers indicate percentages. Data are from one experiment representative of two experiments. Error bars indicate SD. *P < 0.05, **P < 0.01, *** P < 0.001, **** P < 0.0001, ordinary one-way Anova with Dunnett's post hoc test in **A, C-E**. ns; not significant.

To study CTL priming, we next performed opt-SNE analysis of $CD8^+$ T cells with a $CD44^+$ $CD62L^-$ effector phenotype found in the TdLN. The flow cytometry panel included the marker TCF-1 to monitor CTL effector differentiation, which progresses over a continuum of cellular states depending on the input signals delivered[60,61]. Loss of TCF-1 expression (a transcription factor encoded by *Tcf7*) is associated with loss of "stemness"[62] and highlights T cells that are on the path of becoming terminally differentiated short-lived effector T cells[63]. Contour plot visualization showed significant enlargement of a $TCF\text{-}1^-$ subpopulation among $CD44^+$ $CD62L^-$ cells in the TdLN upon RT, which was further increased upon CD86, but not CD80 blockade (Figure **6E,F**). Manual gating (Figure **S5D**) confirmed these findings and showed that CD86 blockade in the context of RT significantly increased the frequency of $CD44^+$ $TCF\text{-}1^-$ cells among $CD8^+$ T cells in both TdLN and tumor (Figure **6G**). In concordance, phenotypical analysis showed increased expression of the (terminal) effector differentiation markers CD43, CX3CR1, GZB and KLRG1 on the $CD44^+$ $TCF\text{-}1^-$ population as compared to the $CD44^+$ $TCF\text{-}1^+$ population (Figure **6H**). Moreover, the $CD44^+$ $TCF\text{-}1^-$ population also showed enhanced Ki67 expression, indicating increased cell cycle activity (Figure **6H**). Taken together, these findings indicate that CD86 blockade improves RT-induced CTL priming, expansion and effector differentiation, likely mediated by enhanced cDC1 presence and activity in the TdLN.

RT plus PD-1 blockade increases the Treg response, which is overruled by CD86 blockade resulting in improved tumor control.

PD-1, the key target in current cancer immunotherapy, is considered a hallmark of suboptimally primed CTLs that lack full cytotoxic effector functions[64,65]. Further analysis of the $CD44^+$ $TCF\text{-}1^-$ population in the tumor after combined RT and CD86 blockade, showed that these cells expressed PD-1, albeit to a lesser extent than the less differentiated $CD44^+$ $TCF\text{-}1^+$ cells (Figure **S6A**). In fact, we observed that in the tumor, both eTregs and the $Ki67^+$ CTLs expressed PD-1 (Figure **7A**). PD-1 inhibits CD28 costimulation[19], which is valid for both Tconvs and Tregs. Recent reports describe that in addition to supporting Tconv responses[64,65], PD-1 blockade may also promote Treg responses by enabling TCR/CD28 signaling[66,67]. Therefore, we examined the effect of PD-1 blockade alone, or in combination with CD86 blockade on the RT-induced Treg and CTL response. Strikingly, PD-1 blockade increased RT-induced eTreg priming and tumor infiltration, while these responses were inhibited upon CD86 blockade, as we observed before (Figure **7B,C**, Figure **S6B,C**). Following combined PD-1 and CD86 blockade, the RT-induced eTreg response was abrogated as it was upon CD86 blockade alone, confirming that CD86 is the key driver of the eTreg response. Importantly, following combined PD-1 and CD86 blockade, the RT-induced CTL response was significantly increased in TdLN and tumor (Figure **7B**,**D**, Figure **S6B,C**). These results agree with the concept that RT-induced Treg priming hampers the induction of a CTL response, as we showed before.

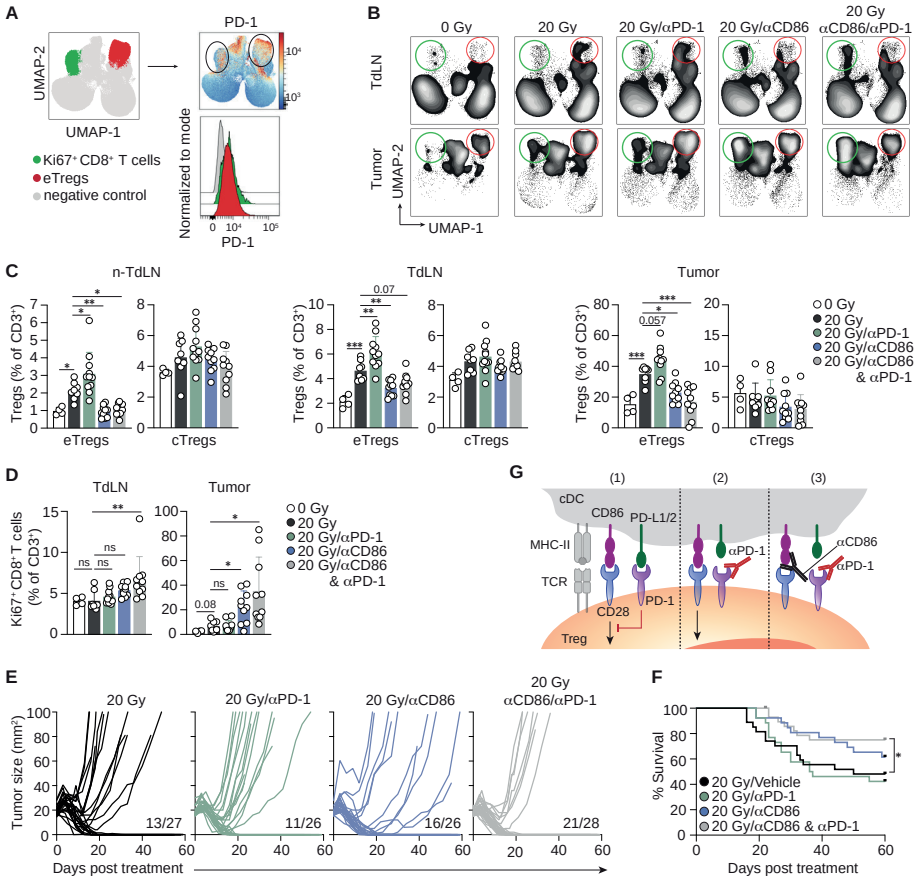

Figure 7. CD86-mediated CD28 costimulation is required for PD-1-dependent eTreg expansion.
(**A**) PD-1 protein expression of the Ki67$^+$ CD8$^+$ T cell population (green) and eTreg population (red) in the tumor identified in Figure **5A**, depicted as heatmap (upper row) and representative histogram (lower row) of all experimental settings combined. (**B,C**) Mice bearing TC-1 tumors received control treatment (0 Gy, n=4) or 20 Gy RT at day 0 in combination with either vehicle (PBS, n=8) or blocking mAb against PD-1 (n=11), CD86 (n=10) or a combination of both (n = 10) at day 0, 3 and 6. The CD3$^+$ lymphocyte response was monitored by flow cytometry in the non-TdLN, TdLN and tumor at day 8. (**B**) UMAP visualization of the response of the CD3$^+$ subpopulation in TdLN and tumor to the indicated treatments. The red circle highlights the eTreg population, whereas the green circle indicates the Ki67$^+$ CD8$^+$ T cells (see also Figure **S6A,B**). (**C**) Frequencies of eTregs and cTregs identified in Figure **S6A** among CD3$^+$ cells found in the indicated tissues at day 8 post treatment. (**D**) Quantification of the Ki67$^+$ CD8$^+$ T cell population among total CD3$^+$ cells in the TdLN and tumor at day 8 post treatment. (**E**) Individual tumor growth curves (**F**) and overall survival of mice bearing TC-1 tumors receiving RT at day 0 in combination with either vehicle (PBS, n=27) or blocking mAb against PD-1 (n=26), CD86 (n=26) or a combination of both (n=28) at dat 0, 3 and 6. Ratios indicate the number of mice that showed full recovery upon treatment compared to total. (**G**) Illustration depicting the proposed mechanism of action of combined CD86 and PD-1 blockade on Tregs in our setting. (1) PD-L1/L2 offered by dendritic cells (cDCs) ligates PD-1 and prevents downstream signaling of CD28 on Tregs. (2) PD-1 blockade negates this process, resulting in enhanced CD28 costimulation and consequently increased Treg cellular responses. (3) When CD86 blockade is in place, CD28 costimulation is prevented, and additional PD-1 blockade can no longer engage the CD28 costimulatory axis, resulting in an abrogated Treg response. Data are from one experiment representative of two experiments. Error bars indicate SD. *P < 0.05, **P < 0.01, *** P < 0.001, ordinary one-way Anova with Dunnett's post hoc test in **C**; Brown-Forsythe Anova with Dunnett's T3 post hoc analysis in **D**; Mantel-Cox analysis in **F**. ns; no significance.

We next assessed how inhibition of PD-1 and/or CD86 impacted RT-induced tumor control. PD-1 blockade alone failed to enhance RT-induced tumor regression and overall survival, in line with stimulation of the Treg response (Figure **7E,F**, Figure **S6D**). CD86 blockade alone initially improved RT-induced tumor control, but a fraction of these tumors eventually relapsed. Combined PD-1 and CD86 blockade cured 75% of the mice and significantly increased overall survival compared to RT alone. However, combined PD-1 and CD86 blockade did not increase the therapeutic effect as compared to CD86 blockade alone, confirming that CD86 inhibition is the primary factor to alleviate Treg-obstructed RT-induced CTL-mediated tumor control. Taken together, these data indicate that in this lymphocyte-depleted tumor model, RT enhances eTreg priming while restraining tumor-reactive CTL priming and this is further enhanced by PD-1 blockade. This result can be explained by the fact that PD-1 blockade preferentially enables CD28 costimulation on Tregs (Figure **7G**). CD86, but not CD80 blockade, counteracts Treg priming through inhibition of CD28 costimulation and thereby facilitates tumor-reactive CTL priming and tumor control by RT.

Discussion

The potential of RT to induce systemic T-cell responses to cancer has recently received much attention, but clinical evidence for abscopal, immune-mediated effects are scarce, even in combination with ICB[6]. We must therefore better understand the ability of RT to induce tumor-controlling T-cell responses, in the context of the divergent impact of different cancer types on the immune response. Comparison of *in vivo* tumor models of varying immunogenicity demonstrated that in immunogenic tumors, $CD8^+$ T cells infiltrating the TME contributed to the RT response, while in poorly immunogenic tumors RT failed to elicit a systemic anti-tumor immune response and an abscopal effect[18]. We show that the TC-1 tumor model used in our current study recapitulates a "lymphocyte depleted" phenotype represented among human cancer types[3] that proves to respond negatively to RT (Figure **1A**). Despite expression of HPV-16 derived E6 and E7 antigens, the TC-1 tumor contains a very low amount of Tconvs and primarily contain myeloid populations. We show that the TC-1 tumor invites Tregs and monocytes in the tumor and the TdLN, consistent with systemic immunosuppression, as observed in this type of tumors in the clinic[68,69]. Nevertheless, the RT response was $CD8^+$ T-cell dependent, suggesting that in lymphocyte-depleted tumors, there is an unexploited, favorable T-cell response that should be improved by the correct intervention(s).

To prime CTLs, cDC1s need to be activated and migrate to the TdLN[54,55], whereas the cDC2 subset is particularly effective at $CD4^+$ T-cell priming, including both Tconvs and Tregs[56,70]. In the TC-1 tumor setting, RT induced new CTL priming, despite concurrent Treg priming. This suggests that RT produced DAMPs required to activate cDC1s and induced their migration to the TdLN. However, as RT may upregulate signals that prevent cDC1 recruitment to the TME[71], CTL priming in the TC-1 setting may be limited by the number of cDC1s present in the tumor before RT, which was very

low (Figure **2A**). As TC-1 has a much higher proportion of cDC2s, cDC2-induced Treg priming may therefore dominate over cDC1-induced CTL priming in the TdLN after RT.

A main role for Tregs lies in prevention or suppression of unwanted Tconv responses against both self- and foreign-antigens[72]. At steady state, "immature" or "tolerogenic" cDCs that express CD86 but no other costimulatory ligands[73] migrate from peripheral tissues to dLNs to present self-antigens and prevent responses of sporadic, autoreactive T cells. This role is exerted by cTregs that do not show extensive clonal expansion or relocation to non-lymphoid tissues. A recent study reports that Treg priming may be dictated by the metabolic state of cDC2s, in part through CD86 upregulation, required to promote Treg expansion[74]. Especially in a tumor setting, limited nutrient resources in conjunction with tumor-associated immunosuppressive factors may induce a metabolic state in cDCs that supports Treg priming and/or expansion[75].

In a tumor setting, Treg accumulation in the TdLN can restrict CTL priming by inhibiting cDC1 activation in the TdLN[76]. CD86 blockade in our model effectively reduced RT-induced eTreg responses, while concurrently increasing the presence of cDC1 cells in the TdLN and enhancing their expression of both CD80 and PD-L1. This enhanced expression is favorable for the formation of a CD28-costimulatory CD80/PD-L1 heterodimer. Accordingly, CD86 blockade selectively improved the CTL response following RT. Based on these data, it is likely that the RT-induced eTreg response in the TdLN in part prevents CTL priming by limiting cDC1 availability and functionality.

Tregs play a role in controlling inflammation resulting from tissue injury, such as inflicted by RT. In this process, cTregs are recruited from dLNs to damaged tissues[77], where they present an effector (eTreg) phenotype[21]. Murine and human tissue-resident eTregs have a conserved transcriptional signature that is most explicit in tumor-resident eTregs and contains a tissue-repair program[78]. In an irradiated tumor, next to extinguishing inflammatory responses, these eTregs may utilize their repair function to support extracellular matrix remodeling and tumor growth[79] and therefore may form an impediment to RT efficacy.

In our setting, CD86, but not CD80, drove induction of an eTreg response by RT. In principle, both Tconvs and Tregs can profit from either CD80 or CD86 to receive CD28 costimulation. However, on Tregs, constitutively expressed CTLA-4 imposes an intrinsic constraint for CD28 costimulation. Since CD86 has a lower affinity for CTLA-4 than CD80, it has improved accessibility for CD28 on Tregs and therefore Tregs selectively profit from CD86 costimulation[80]. Upon CTLA-4 blockade, both CD80 and CD86 are available to support the Treg response[50], especially in our tumor setting where the Treg response is dominant. Interestingly, blockade of CTLA-4 together with RT supported both cTreg and eTreg expansion, whereas RT alone induced an eTreg response. Thus, CTLA-4 inhibition led to CD28 costimulation and consequent expansion of cTregs, while additional signals induced by RT promoted eTreg differentiation.

In certain mouse tumor models (TSA and 4T1 breast cancer and MCA38 colon cancer), CTLA-4 blockade and RT have a combined therapeutic effect[26,39,47,48]. CTLA-4 likely promoted new T-cell priming in these models, given the increased TCR diversity of tumor-infiltrating T cells observed. Such a combined effect was also found in subsets of patients with metastatic non-small cell lung cancer[26] or metastatic melanoma[25]. In the TC-1 model, however, there was no added therapeutic effect of CTLA-4 blockade to RT, which was explained by increased Treg over CTL priming. It is known that CTLA-4 ICB efficacy largely relies on a high CTL over Treg ratio in the tumor[81,82], highlighting that CTLA-4 blockade must favor CTL over Treg priming in this setting[82]. In T-cell depleted tumors, several factors work against a favorable CTL over Treg ratio, e.g. a higher cDC2-over cDC1 ratio in the TME, limited RT-induced adjuvanticity[31] and/or RT-induced suppressive factors that prevent cDC1 maturation[71,83]. Reportedly, fractionated low dose RT is superior in eliciting IFN-I dependent optimization of cDC1 for CTL priming. This is because single high dose RT attenuates IFN-I release by promoting DNA degradation via the exonuclease Trex1[39]. Consequently, 3x8 Gy, but not 20 Gy, cooperated with CTLA-4 blockade to improve systemic anti-tumor immunity in TSA and 4T1 mouse models[26,39,47,48]. However, in our model, RT induced a strong Treg response to both 3x 8 Gy and 20 Gy and these schedules had no differential therapeutic effect. Thus, in Treg dominant tumors, CTLA-4 blockade may preferentially support Treg expansion[84] and not improve CTL-based tumor control, regardless of the RT regimen used[44,85].

In our tumor setting, PD-1 blockade also exacerbated the RT-induced eTreg response and consequently impeded the therapeutic CTL response. Importantly, it was recently reported that PD-1 blockade can promote Treg responses in cancer patients, which can lead to cancer hyper-progression[66,86]. These studies showed that both Tregs and Tconvs can profit from CD28 costimulation that is enabled by PD-1 blockade[19]. In tumors that favor Treg- over CTL priming at steady state and that have an exacerbated eTreg response upon RT, the conditions are met for further Treg priming and expansion upon PD-1 blockade. Our discovery that CD86 blockade abrogated the Treg response in this setting is therefore of potential clinical relevance. When CD86 was blocked, PD-1 blockade could not induce Treg expansion upon RT, indicating its dependence on CD86-mediated CD28 costimulation. Importantly, CTL priming depended on CD80-mediated costimulation and was not affected by CD86 blockade, allowing for reversal of the Treg/CTL ratio.

In conclusion, we reveal that in a model of lymphocyte-depleted cancer that favors myeloid and Treg infiltration, CTLA-4 and PD-1 blockade have the opposite effect on RT-induced tumor control than in immunogenic tumors with high Tconv infiltrates. This is due to exacerbation of RT-induced Treg responses that counteract the RT-induced CTL response. We therefore caution that CTLA-4 and/or PD-(L)1 blockade may likewise exacerbate RT-induced Treg responses in human lymphocyte-depleted cancer. Our findings argue that instead, CD86 is a suitable target to inhibit undesired Treg responses and a new candidate to improve Tconv cell responses to poorly immunogenic cancers, particularly in combination with RT.

Methods

TCGA data analysis

Immune subtype classifications among 9126 tumors were collected from Thorsson et al.[3]. Patient-specific radiotherapy status and survival metrics were gathered from the UCSC Xena Platform using the *UCSCXenaTools* package[87] of which 7891 tumors had complete information available. Following this, Kaplan-Meier curves were generated for each immune subtype using overall survival (in months) by radiotherapy status (yes vs. no). For the immune subtype prediction, the C4/C5 subtypes were first collapsed into a single immune subtype and tumors derived from the C3 and C4/C5 immune subtypes were selected (n=3939). Following this, features derived from the CIBERSORT deconvolution algorithm and IFNγ signature were subsequently used (n=23). Next, 70% and 30% of the data was split into training and testing datasets, respectively. The training data was first scaled and centered before undergoing a 5-fold repeated cross-validation strategy to predict between C4/C5 vs. C3 using a K-nearest neighbor (KNN) model. The test data was then applied to evaluate model performance.

Murine microarray analysis

Microarray data and metadata was downloaded from *GSE85509* using *GEOquery.* Murine gene symbols were converted to human symbols using the *biomaRt* package. Following this, immune cell types were deconvolved using *CIBERSORT* from the *immunedeconv* package and the IFNγ signature was generated using the Ayers gene signature[88]. Next, the data from the TC-1 and MC38 cell lines were used as input into the trained KNN model for classification.

Tumor cells

The MC38 colon cancer cell line was purchased from Kerafast (Boston, MA) and TC-1 tumor cells (lung epithelial cells engineered to express HPV16 E6 and E7 proteins[35]) were obtained from Leiden University Medical Center in 2015 and the authors did not perform further authentication. MC38 and TC-1 cells were cultured in DMEM and RPMI 1640 (Gibco, Life Technologies) respectively, supplemented with 10% fetal calf serum (FCS), 0.1 mM non-essential amino acids, 1 mM sodium pyruvate, 2 mM L-glutamine, 10 mM HEPES and penicillin/streptomycin (Roche) at 37°C, 5% CO_2. MC38 and TC-1 cell stocks were tested negative for *Mycoplasma* by PCR, and thawed cells were used within 3 passages for *in vivo* experiments.

Tumor transplantation and RT

Six- to eight-week-old female C57BL/6Rj (B6) mice were purchased from Janvier Laboratories (Le Genest Saint Isle, France). At day -8, mice were anesthetized with isofluorane and injected subcutaneously (s.c.) with either $1x10^6$ MC38 or $1x10^5$ TC-1 tumor cells in 50 µl HBSS. Tumor size

was measured by calipers in two dimensions and calculated as: area (mm^2) = width x length. RT was initiated when the tumors reached 18-25 mm^2 (indicated as day 0) and mice were randomly assigned to different treatment groups. RT was applied using the SmART$^+$ system (Precision X-Ray, North Branford, CT). Mice were anesthetized with isoflurane and a cone-beam CT scan of the mice was performed. The tumor was localized on the CT scan and targeted with RT at 0.1 mm precision using round collimators 1.0 or 1.5 cm in diameter. A single fraction of 8 or 20 Gy (225 peak kilovoltage (kVp), filtered with 0.3 mm of copper (3 Gy/min)) was delivered. For fractionated dosage studies, a single dose of 8 Gy was delivered on days 0, 1 and 2. Control mice (indicated as 0 Gy) were anesthetized and received a cone-beam CT scan but were not exposed to RT. Mice were sacrificed when the tumor diameter reached 15 mm or when the tumor size reached >100 mm^2. In the survival curves, censored events indicate mice that were sacrificed due to treatment unrelated disease.

Therapeutic antibodies and reagents

Mice received intraperitoneal (i.p.) injections of depleting anti-CD8α-mAb (2.43, BioXCell) or anti-CD4-mAb (GK1.5, BioXCell) at 200 µg per mouse in 100 µl PBS starting at day -1 prior to RT (day 0) followed by days 3, 6 and 9. For Treg depletion experiments, mice were injected i.p. with 250 µg of depleting mouse IgG2a isotype CD25-mAb[46] (modified clone of PC61, Evitria) in 100 µl PBS at day -1 prior to RT and at day 5. Blocking mAbs to CTLA-4 (UC10-4F10-11, BioXCell), PD-1 (RMP1-14, BioXCell), CD80 (1G10, BioXCell) and CD86 (GL-1, BioXCell) were injected i.p. at either 100 µg (anti-CTLA-4 and anti-PD-1) or 200 µg (anti-CD80 and anti-CD86) per mouse in 100 µl PBS at the day of RT (day 0) and days 3, 6, and in case of anti-CTLA-4 also at day 9. Control mice were injected with equal amounts of PBS (vehicle) according to the treatment schedule indicated. The sphingosine-1-phosphate receptor-1 agonist FTY720 (Fingolimod; Cayman Chemical) was dissolved in 0.9% NaCl solution (vehicle) and administered at 2 mg/kg by oral gavage. FTY720 treatment started one day prior to RT and was repeated three times per week throughout the duration of the experiment. All treatments were administered at standardized time points to correct for fluctuations in the adaptive immune response influenced by circadian oscillations[89].

Tissue preparation and flow cytometry

At the indicated time points, tumor-bearing mice were sacrificed, and the lymphoid tissues and tumors were isolated. We performed intra-tumoral injection of 5% Evans Blue dye (Sigma-Aldrich) in 50 µl PBS to identify the axillary LN on the tumor bearing side as the TdLN, whereas the contralateral inguinal LN was defined as the non-TdLN. The TdLN was carefully kept out of the field of irradiation to prevent RT-induced attenuation of the adaptive immune responses in the LN[90]. Tumor tissue was mechanically disaggregated using a McIlwain tissue chopper (Mickle Laboratory Engineering), and a single-cell suspension was prepared by digesting the tissue in collagenase type A (Roche) and 25

µg/ml DNase I (Sigma) in serum-free DMEM for 45 min at 37°C. Enzyme activity was neutralized by addition of medium containing 10% FCS, and the tissue was dispersed by passing through a 70-µm cell strainer. To acquire single cell suspensions of LNs, the tissue was punctured with a 27 G needle followed by incubation in 100 µg/mL Liberase™ TL (Roche) in serum-free DMEM for 30 min at 37°C. Enzyme activity was neutralized as described above and tissue was dispersed by passing through a 70-µm cell strainer. Peripheral blood cells were collected from tail blood of live mice in Microvette CB300 LH tubes (Sarstedt). Red blood cells were lysed in 0.14 M NH_4Cl and 0.017 M Tris-HCl (pH 7.2) for 1 min at room temperature and cell suspensions were washed and stained with relevant mAbs (Table 1). For surface staining, single cells of the isolated tissues were first incubated with anti-CD16/32 (1:50, clone 2.4G2, BD Bioscience) supplemented with 10 µg/ml DNAse, to block unspecific Fc receptor binding, for 10 min on ice. Next, surface antibody staining was performed (Table 1) for 30 min in PBS containing 0.5% BSA and 0.01% sodium azide. For intracellular staining of transcription factors and cytokines, cells were fixed and permeabilized with the FOXP3 Transcription Factor Staining Buffer Set according to the manufacturer's protocol (Thermo Fischer Scientific). Dead cells were excluded by using Fixable Viability Near-infra red dye (1:1000, Life Technologies), Zombie Red Fixable Viability Kit (1:5000, BioLegend) or Zombie UV fixable viability Kit (1:500, BioLegend). Cytokine detection in tumor and lymph node single cell preparations was performed following *ex vivo* stimulation in presence of 1 µg/ml GolgiPlug (BD Biosciences) with 50 ng/ml phorbol 12-myristate 13-acetate (PMA, Sigma Aldrich) and 1 µM ionomycin (Sigma Aldrich) dissolved in DMSO and diluted in 100 µl IMDM containing 8% FCS for 3 h at 37°C, 5% CO_2. Control (unstimulated) cells were treated with an equal volume of DMSO in presence of GolgiPlug diluted in IMDM with 8% FCS. Absolute cell numbers were determined by adding AccuCount Blank Particles (7-7.9 µm, Spherotech) to each sample, prior to flow cytometry analysis. Fluorescence minus one (FMO) was used as a negative control for activation markers. Flow cytometry was performed using a BD FACSymphony™ A5 SORP flow cytometer or the 5-laser Cytek Aurora. All generated data was analyzed using FlowJo and OMIQ software (Dotmatics, Boston, MA).

Data analysis

Dimensionality reduction and FlowSOM[91] analysis of flow cytometry data was performed using OMIQ software. Following conventional marker expression analysis, the population of interest was manually gated, and down-sampling was performed to select the maximal number of cells per tissue representative for all tissue types included, as indicated in the figure legends. Tumor samples containing <600 cells of the subsampled population were excluded from further analysis (see Figure **5D**). K-means clustering of the indicated populations was performed using FlowSOM, including all markers indicated, except for live/dead and CD45 and in case of the $CD8^+$ T cell population (see Figure **6E,F**) also without CD3. Dimension reduction and visualization was performed using uniform manifold approximation and projection (UMAP) analysis[92] and opt-SNE analysis[93], including the same markers as described above and by using the default OMIQ settings.

Statistical analysis

All statistical data were analyzed using GraphPad Prism version 9 (GraphPad Software, La Jolla, CA). Statistical analyses were performed as indicated in the figure legends. Ordinary one-way Anova was performed in case sample sizes were $n>8$, more than three experimental groups were compared and if the assumption for normal distribution was met. In case sample sizes were $n<8$ and if normal distribution could not be assumed, Kruskal-Wallis analysis was applied. A P value <0.05 was considered statistically significant; *$p<0.05$, **$p<0.01$, ***$p<0.001$, ****$p<0.0001$. Data are presented as mean + S.D.

Study approval

Mice were maintained in individually ventilated cages (Innovive, San Diego, CA) under specific pathogen-free conditions. All mouse experiments were performed in accordance with institutional and national guidelines and were approved by the Animal Welfare Body (IVD) of the Netherlands Cancer Institute.

Author contributions

Conception and design: E.F., J. Bo.
Development of methodology: E.F., T.W.B., I.V.
Experimental advice: D.M.T.B., T.W.B., J. Bu., M.D.S., I.V.
Acquisition of data: E.F., D.M.T.B., T.W.B., J. Bu., M.D.S.
Analysis and interpretation of data: E.F., T.W.B., J. Bo.
Writing of manuscript: E.F., J.Bo.
Critical reading and editing of the paper: D.M.T.B., T.W.B., J. Bu., M.D.S., I.V.

Acknowledgements

We thank dr. Ramon Arens for providing the CD80 and CD86 blocking antibodies, and dr. Sergio Quezada for providing the CD25 IgG2a *in vivo* depletion antibody. We thank all members of the Immunology department at LUMC, and all members of the Tumor Biology & Immunology department at NKI, for their insightful input and helpful discussions. We thank the flow cytometry facility, animal laboratory facility and the intervention unit of the Netherlands Cancer Institute for technical assistance. This work was supported by the Dutch Cancer Society Grant NKI 2017-10894 to I. Verbrugge and J. Borst.

Conflict of Interest:

The authors declare no competing interests.

References

1 Haslam, A. & Prasad, V. Estimation of the Percentage of US Patients With Cancer Who Are Eligible for and Respond to Checkpoint Inhibitor Immunotherapy Drugs. *JAMA Netw Open* **2**, e192535 (2019).

2 Huang, A. C. *et al.* T-cell invigoration to tumour burden ratio associated with anti-PD-1 response. *Nature* **545**, 60-65 (2017).

3 Thorsson, V. *et al.* The Immune Landscape of Cancer. *Immunity* **48**, 812-830 e814 (2018).

4 Luca, B. A. *et al.* Atlas of clinically distinct cell states and ecosystems across human solid tumors. *Cell* **184**, 5482-5496 e5428 (2021).

5 Chen, D. S. & Mellman, I. Elements of cancer immunity and the cancer-immune set point. *Nature* **541**, 321-330 (2017).

6 Pointer, K. B., Pitroda, S. P. & Weichselbaum, R. R. Radiotherapy and immunotherapy: open questions and future strategies. *Trends Cancer* **8**, 9-20 (2022).

7 Kroon, P. *et al.* Radiotherapy and Cisplatin Increase Immunotherapy Efficacy by Enabling Local and Systemic Intratumoral T-cell Activity. *Cancer Immunol Res* **7**, 670-682 (2019).

8 Formenti, S. C. & Demaria, S. Systemic effects of local radiotherapy. *Lancet Oncol* **10**, 718-726 (2009).

9 Lee, Y. *et al.* Therapeutic effects of ablative radiation on local tumor require CD8+ T cells: changing strategies for cancer treatment. *Blood* **114**, 589-595 (2009).

10 Takeshima, T. *et al.* Local radiation therapy inhibits tumor growth through the generation of tumor-specific CTL: its potentiation by combination with Th1 cell therapy. *Cancer Res* **70**, 2697-2706 (2010).

11 Lugade, A. A. *et al.* Local radiation therapy of B16 melanoma tumors increases the generation of tumor antigen-specific effector cells that traffic to the tumor. *J Immunol* **174**, 7516-7523 (2005).

12 Kroemer, G., Galassi, C., Zitvogel, L. & Galluzzi, L. Immunogenic cell stress and death. *Nat Immunol* **23**, 487-500 (2022).

13 Golden, E. B. & Apetoh, L. Radiotherapy and immunogenic cell death. *Semin Radiat Oncol* **25**, 11-17 (2015).

14 Bottcher, J. P. & Reis e Sousa, C. The Role of Type 1 Conventional Dendritic Cells in Cancer Immunity. *Trends Cancer* **4**, 784-792 (2018).

15 Abuodeh, Y., Venkat, P. & Kim, S. Systematic review of case reports on the abscopal effect. *Curr Probl Cancer* **40**, 25-37 (2016).

16 Demaria, S. *et al.* Ionizing radiation inhibition of distant untreated tumors (abscopal effect) is immune mediated. *Int J Radiat Oncol Biol Phys* **58**, 862-870 (2004).

17 Buchwald, Z. S. *et al.* Tumor-draining lymph node is important for a robust abscopal effect stimulated by radiotherapy. *J Immunother Cancer* **8** (2020).

18 Lai, J. Z. *et al.* Abscopal Effects of Local Radiotherapy Are Dependent on Tumor Immunogenicity. *Front Oncol* **11**, 690188 (2021).

19 Hui, E. *et al.* T cell costimulatory receptor CD28 is a primary target for PD-1-mediated inhibition. *Science* **355**, 1428-1433 (2017).

20 Esensten, J. H., Helou, Y. A., Chopra, G., Weiss, A. & Bluestone, J. A. CD28 Costimulation: From Mechanism to Therapy. *Immunity* **44**, 973-988 (2016).

21 Smigiel, K. S. *et al.* CCR7 provides localized access to IL-2 and defines homeostatically distinct regulatory T cell subsets. *J Exp Med* **211**, 121-136 (2014).

22 Simpson, T. R. *et al.* Fc-dependent depletion of tumor-infiltrating regulatory T cells co-defines the efficacy of anti-CTLA-4 therapy against melanoma. *J Exp Med* **210**, 1695-1710 (2013).

23 Wing, K. *et al.* CTLA-4 control over Foxp3+ regulatory T cell function. *Science* **322**, 271-275 (2008).

24 Voorwerk, L. *et al.* Immune induction strategies in metastatic triple-negative breast cancer to enhance the sensitivity to PD-1 blockade: the TONIC trial. *Nat Med* **25**, 920-928 (2019).

25 Twyman-Saint Victor, C. *et al.* Radiation and dual checkpoint blockade activate non-redundant immune mechanisms in cancer. *Nature* **520**, 373-377 (2015).

26 Formenti, S. C. *et al.* Radiotherapy induces responses of lung cancer to CTLA-4 blockade. *Nat Med* **24**, 1845-1851 (2018).

27 Theelen, W. *et al.* Effect of Pembrolizumab After Stereotactic Body Radiotherapy vs Pembrolizumab Alone on Tumor Response in Patients With Advanced Non-Small Cell Lung Cancer: Results of the PEMBRO-RT Phase 2 Randomized Clinical Trial. *JAMA Oncol* **5**, 1276-1282 (2019).

28 Arina, A. *et al.* Tumor-reprogrammed resident T cells resist radiation to control tumors. *Nat Commun* **10**, 3959 (2019).

29 Crittenden, M. R. *et al.* Tumor cure by radiation therapy and checkpoint inhibitors depends on pre-existing immunity. *Sci Rep* **8**, 7012 (2018).

30 Blair, T. C. *et al.* Dendritic Cell Maturation Defines Immunological Responsiveness of Tumors to Radiation Therapy. *J Immunol* **204**, 3416-3424 (2020).

31 Blair, T. C. *et al.* Fluorescent tracking identifies key migratory dendritic cells in the lymph node after radiotherapy. *Life Sci Alliance* **5** (2022).

32 Mondini, M. *et al.* CCR2-Dependent Recruitment of Tregs and Monocytes Following Radiotherapy Is Associated with TNFalpha-Mediated Resistance. *Cancer Immunol Res* **7**, 376-387 (2019).

33 Mosely, S. I. *et al.* Rational Selection of Syngeneic Preclinical Tumor Models for Immunotherapeutic Drug Discovery. *Cancer Immunol Res* **5**, 29-41 (2017).

34 Hos, B. J. *et al.* Identification of a neo-epitope dominating endogenous CD8 T cell responses to MC-38 colorectal cancer. *Oncoimmunology* **9**, 1673125 (2019).

35 Lin, K. Y. *et al.* Treatment of established tumors with a novel vaccine that enhances major histocompatibility class II presentation of tumor antigen. *Cancer Res* **56**, 21-26 (1996).

36 Ahrends, T. *et al.* CD4(+) T Cell Help Confers a Cytotoxic T Cell Effector Program Including Coinhibitory Receptor Downregulation and Increased Tissue Invasiveness. *Immunity* **47**, 848-861 e845 (2017).

37 Perez-Ruiz, E. *et al.* Prophylactic TNF blockade uncouples efficacy and toxicity in dual CTLA-4 and PD-1 immunotherapy. *Nature* **569**, 428-432 (2019).

38 Ahrends, T. *et al.* CD27 Agonism Plus PD-1 Blockade Recapitulates CD4+ T-cell Help in Therapeutic Anticancer Vaccination. *Cancer Res* **76**, 2921-2931 (2016).

39 Vanpouille-Box, C. *et al.* DNA exonuclease Trex1 regulates radiotherapy-induced tumour immunogenicity. *Nat Commun* **8**, 15618 (2017).

40 Hiam-Galvez, K. J., Allen, B. M. & Spitzer, M. H. Systemic immunity in cancer. *Nat Rev Cancer* **21**, 345-359 (2021).

41 Bauer, C. A. *et al.* Dynamic Treg interactions with intratumoral APCs promote local CTL dysfunction. *J Clin Invest* **124**, 2425-2440 (2014).

42 Matloubian, M. *et al.* Lymphocyte egress from thymus and peripheral lymphoid organs is dependent on S1P receptor 1. *Nature* **427**, 355-360 (2004).

43 Muroyama, Y. *et al.* Stereotactic Radiotherapy Increases Functionally Suppressive Regulatory T Cells in the Tumor Microenvironment. *Cancer Immunol Res* **5**, 992-1004 (2017).

44 Ji, D. *et al.* Combination of radiotherapy and suppression of Tregs enhances abscopal antitumor effect and inhibits metastasis in rectal cancer. *J Immunother Cancer* **8** (2020).

45 Sainz-Perez, A., Lim, A., Lemercier, B. & Leclerc, C. The T-cell receptor repertoire of tumor-infiltrating regulatory T lymphocytes is skewed toward public sequences. *Cancer Res* **72**, 3557-3569 (2012).

46 Arce Vargas, F. *et al.* Fc-Optimized Anti-CD25 Depletes Tumor-Infiltrating Regulatory T Cells and Synergizes with PD-1 Blockade to Eradicate Established Tumors. *Immunity* **46**, 577-586 (2017).

47 Dewan, M. Z. *et al.* Fractionated but not single-dose radiotherapy induces an immune-mediated abscopal effect when combined with anti-CTLA-4 antibody. *Clin Cancer Res* **15**, 5379-5388 (2009).

48 Rudqvist, N. P. *et al.* Radiotherapy and CTLA-4 Blockade Shape the TCR Repertoire of Tumor-Infiltrating T Cells. *Cancer Immunol Res* **6**, 139-150 (2018).

49 Postow, M. A. *et al.* Immunologic correlates of the abscopal effect in a patient with melanoma. *N Engl J Med* **366**, 925-931 (2012).

50 Marangoni, F. *et al.* Expansion of tumor-associated Treg cells upon disruption of a CTLA-4-dependent feedback loop. *Cell* **184**, 3998-4015 e3919 (2021).

51 Salomon, B. *et al.* B7/CD28 costimulation is essential for the homeostasis of the CD4+CD25+ immunoregulatory T cells that control autoimmune diabetes. *Immunity* **12**, 431-440 (2000).

52 Marangoni, F. *et al.* Tumor Tolerance-Promoting Function of Regulatory T Cells Is Optimized by CD28, but Strictly Dependent on Calcineurin. *J Immunol* **200**, 3647-3661 (2018).

53 Tai, X., Cowan, M., Feigenbaum, L. & Singer, A. CD28 costimulation of developing thymocytes induces Foxp3 expression and regulatory T cell differentiation independently of interleukin 2. *Nat Immunol* **6**, 152-162 (2005).

54 Broz, M. L. *et al.* Dissecting the tumor myeloid compartment reveals rare activating antigen-presenting cells critical for T cell immunity. *Cancer Cell* **26**, 638-652 (2014).

55 Salmon, H. *et al.* Expansion and Activation of CD103(+) Dendritic Cell Progenitors at the Tumor Site Enhances Tumor Responses to Therapeutic PD-L1 and BRAF Inhibition. *Immunity* **44**, 924-938 (2016).

56 Binnewies, M. *et al.* Unleashing Type-2 Dendritic Cells to Drive Protective Antitumor CD4(+) T Cell Immunity. *Cell* **177**, 556-571 e516 (2019).

57 Sugiura, D. *et al.* Restriction of PD-1 function by cis-PD-L1/CD80 interactions is required for optimal T cell responses. *Science* **364**, 558-566 (2019).

58 Zhao, Y. *et al.* PD-L1:CD80 Cis-Heterodimer Triggers the Co-stimulatory Receptor CD28 While Repressing the Inhibitory PD-1 and CTLA-4 Pathways. *Immunity* **51**, 1059-1073 e1059 (2019).

59 Oh, S. A. *et al.* PD-L1 expression by dendritic cells is a key regulator of T-cell immunity in cancer. *Nat Cancer* **1**, 681-691 (2020).

60 Kaech, S. M. & Cui, W. Transcriptional control of effector and memory CD8+ T cell differentiation. *Nat Rev Immunol* **12**, 749-761 (2012).

61 Busselaar, J., Tian, S., van Eenennaam, H. & Borst, J. Helpless Priming Sends CD8(+) T Cells on the Road to Exhaustion. *Front Immunol* **11**, 592569 (2020).

62 Zhao, X., Shan, Q. & Xue, H. H. TCF1 in T cell immunity: a broadened frontier. *Nat Rev Immunol* **22**, 147-157 (2022).

63 Chen, Z. *et al.* TCF-1-Centered Transcriptional Network Drives an Effector versus Exhausted CD8 T Cell-Fate Decision. *Immunity* **51**, 840-855 e845 (2019).

64 Philip, M. & Schietinger, A. CD8(+) T cell differentiation and dysfunction in cancer. *Nat Rev Immunol* **22**, 209-223 (2022).

65 Dammeijer, F. *et al.* The PD-1/PD-L1-Checkpoint Restrains T cell Immunity in Tumor-Draining Lymph Nodes. *Cancer Cell* **38**, 685-700 e688 (2020).

66 Kumagai, S. *et al.* The PD-1 expression balance between effector and regulatory T cells predicts the clinical efficacy of PD-1 blockade therapies. *Nat Immunol* **21**, 1346-1358 (2020).

67 Tan, C. L. *et al.* PD-1 restraint of regulatory T cell suppressive activity is critical for immune tolerance. *J Exp Med* **218** (2021).

68 Welters, M. J. *et al.* Vaccination during myeloid cell depletion by cancer chemotherapy fosters robust T cell responses. *Sci Transl Med* **8**, 334ra352 (2016).

69 Wang, L. *et al.* Connecting blood and intratumoral T(reg) cell activity in predicting future relapse in breast cancer. *Nat Immunol* **20**, 1220-1230 (2019).

70 Gerner, M. Y., Casey, K. A., Kastenmuller, W. & Germain, R. N. Dendritic cell and antigen dispersal landscapes regulate T cell immunity. *J Exp Med* **214**, 3105-3122 (2017).

71 Wennerberg, E. *et al.* CD73 Blockade Promotes Dendritic Cell Infiltration of Irradiated Tumors and Tumor Rejection. *Cancer Immunol Res* **8**, 465-478 (2020).

72 Vignali, D. A., Collison, L. W. & Workman, C. J. How regulatory T cells work. *Nat Rev Immunol* **8**, 523-532 (2008).

73 Lutz, M. B. & Schuler, G. Immature, semi-mature and fully mature dendritic cells: which signals induce tolerance or immunity? *Trends Immunol* **23**, 445-449 (2002).

74 Pelgrom, L. R. *et al.* LKB1 expressed in dendritic cells governs the development and expansion of thymus-derived regulatory T cells. *Cell Res* **29**, 406-419 (2019).

75 Moller, S. H., Wang, L. & Ho, P. C. Metabolic programming in dendritic cells tailors immune responses and homeostasis. *Cell Mol Immunol* **19**, 370-383 (2022).

76 Zagorulya, M. *et al.* Tissue-specific abundance of interferon-gamma drives regulatory T cells to restrain DC1-mediated priming of cytotoxic T cells against lung cancer. *Immunity* **56**, 386-405 e310 (2023).

77 Li, J., Tan, J., Martino, M. M. & Lui, K. O. Regulatory T-Cells: Potential Regulator of Tissue Repair and Regeneration. *Front Immunol* **9**, 585 (2018).

78 Delacher, M. *et al.* Single-cell chromatin accessibility landscape identifies tissue repair program in human regulatory T cells. *Immunity* **54**, 702-720 e717 (2021).

79 Wirsdorfer, F. & Jendrossek, V. The Role of Lymphocytes in Radiotherapy-Induced Adverse Late Effects in the Lung. *Front Immunol* **7**, 591 (2016).

80 Halliday, N. *et al.* CD86 Is a Selective CD28 Ligand Supporting FoxP3+ Regulatory T Cell Homeostasis in the Presence of High Levels of CTLA-4. *Front Immunol* **11**, 600000 (2020).

81 Liakou, C. I. *et al.* CTLA-4 blockade increases IFNgamma-producing CD4+ICOShi cells to shift the ratio of effector to regulatory T cells in cancer patients. *Proc Natl Acad Sci U S A* **105**, 14987-14992 (2008).

82 Quezada, S. A., Peggs, K. S., Curran, M. A. & Allison, J. P. CTLA4 blockade and GM-CSF combination immunotherapy alters the intratumor balance of effector and regulatory T cells. *J Clin Invest* **116**, 1935-1945 (2006).

83 Hsieh, R. C. *et al.* ATR-mediated CD47 and PD-L1 up-regulation restricts radiotherapy-induced immune priming and abscopal responses in colorectal cancer. *Sci Immunol* **7**, eabl9330 (2022).

84 Kavanagh, B. *et al.* CTLA4 blockade expands FoxP3+ regulatory and activated effector CD4+ T cells in a dose-dependent fashion. *Blood* **112**, 1175-1183 (2008).

85 Balazs, K. *et al.* Radiotherapy-Induced Changes in the Systemic Immune and Inflammation Parameters of Head and Neck Cancer Patients. *Cancers (Basel)* **11** (2019).

86 Kamada, T. *et al.* PD-1(+) regulatory T cells amplified by PD-1 blockade promote hyperprogression of cancer. *Proc Natl Acad Sci U S A* **116**, 9999-10008 (2019).

87 Goldman, M. *et al.* The UCSC Xena platform for public and private cancer genomics data visualization and interpretation. *bioRxiv*, 326470 (2019).

88 Ayers, M. *et al.* IFN-gamma-related mRNA profile predicts clinical response to PD-1 blockade. *J Clin Invest* **127**, 2930-2940 (2017).

89 Cash, E. *et al.* The role of the circadian clock in cancer hallmark acquisition and immune-based cancer therapeutics. *J Exp Clin Cancer Res* **40**, 119 (2021).

90 Marciscano, A. E. *et al.* Elective Nodal Irradiation Attenuates the Combinatorial Efficacy of Stereotactic Radiation Therapy and Immunotherapy. *Clin Cancer Res* **24**, 5058-5071 (2018).

91 Van Gassen, S. *et al.* FlowSOM: Using self-organizing maps for visualization and interpretation of cytometry data. *Cytometry A* **87**, 636-645 (2015).

92 Becht, E. *et al.* Dimensionality reduction for visualizing single-cell data using UMAP. *Nat Biotechnol* **37**, 38-44 (2018).

93 Belkina, A. C. *et al.* Automated optimized parameters for T-distributed stochastic neighbor embedding improve visualization and analysis of large datasets. *Nat Commun* **10**, 5415 (2019).

Supplementary Data

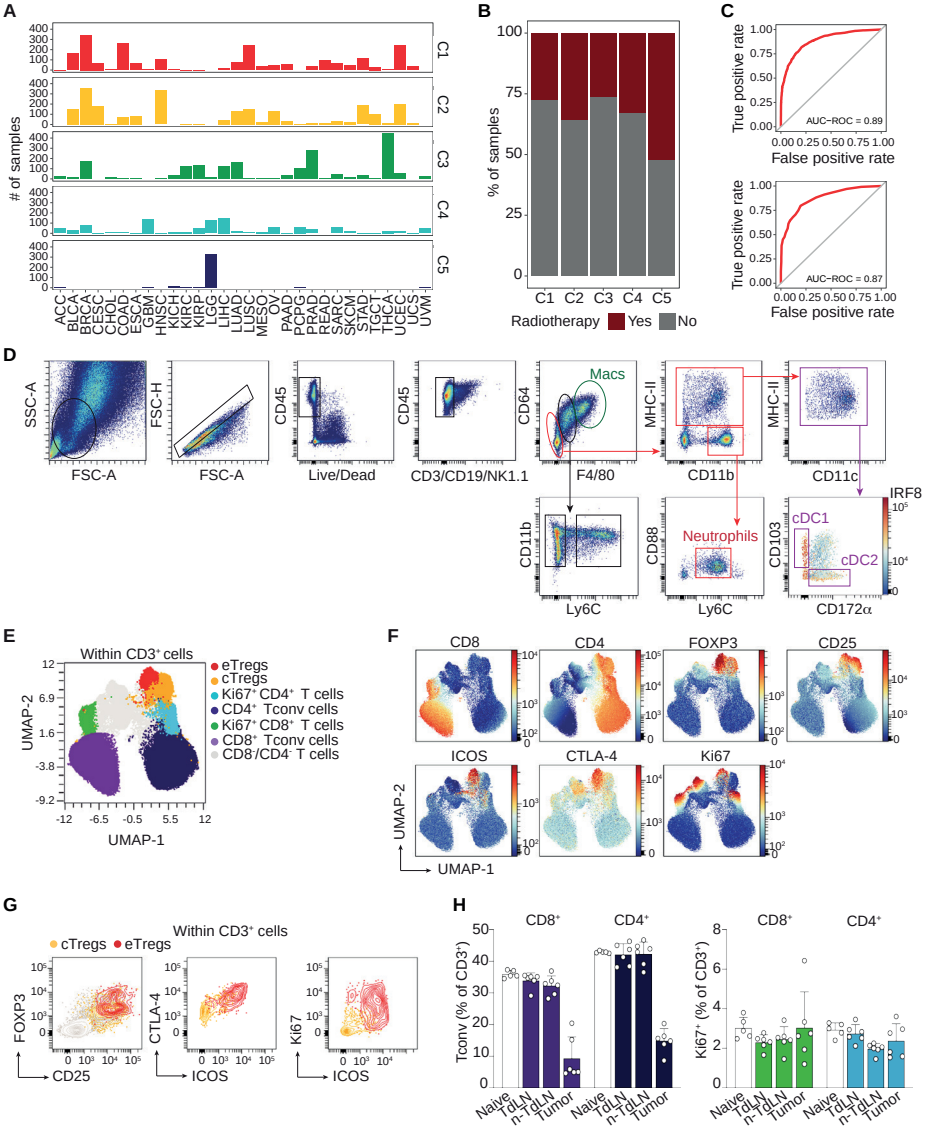

← Supplemental Figure 1- Related to Figure 1 (A – B) and Figure 2 (A – D)
(**A**) Number of TCGA tumor types (for tumor type abbreviation, see Table 2) classified per immune subtype, among tumors for which RT treatment (yes or no) was known. The total number of samples per tumor immune subtype (C1-C5) is indicated in Figure **1A**. (**B**) Distribution of samples that received RT (red) or not (grey) for each tumor immune subtype. (**C**) Training (upper panel) and testing (lower panel) receiver operating curves (ROC) and area under the curve (AUC) calculation of a k-nearest neighbor's model training to classify C3 vs. C4/C5 TCGA immune subtypes. Training and testing were split 75% and 25%, respectively. (**D**) Representative gating strategy of the myeloid populations found in 50 mm^2 TC-1 tumors. (**E-F**) UMAP display of 5000 randomly selected $CD3^+$ cells per sample found in non-TdLN, TdLN and tumors at day 8 of all treatment groups combined. FlowSOM guided clustering (**E**) identifying the $CD3^+$ cell populations and (**F**) representative heat map visualization of the markers that identify the $CD3^+$ (T-cell) subpopulations. (**G**) Representative flow cytometry plots overlaying the in (**E**) identified cTreg and eTreg populations. (**H**) Percentage of the in (**E**) identified $CD8^+$ and $CD4^+$ Tconv populations (left) and $Ki67^+CD8^+$ and $Ki67^+CD4^+$ Tconv populations (right) among the $CD3^+$ cells in the indicated tissues. Error bars indicate SD. Data is from one experiment, representative of two experiments.

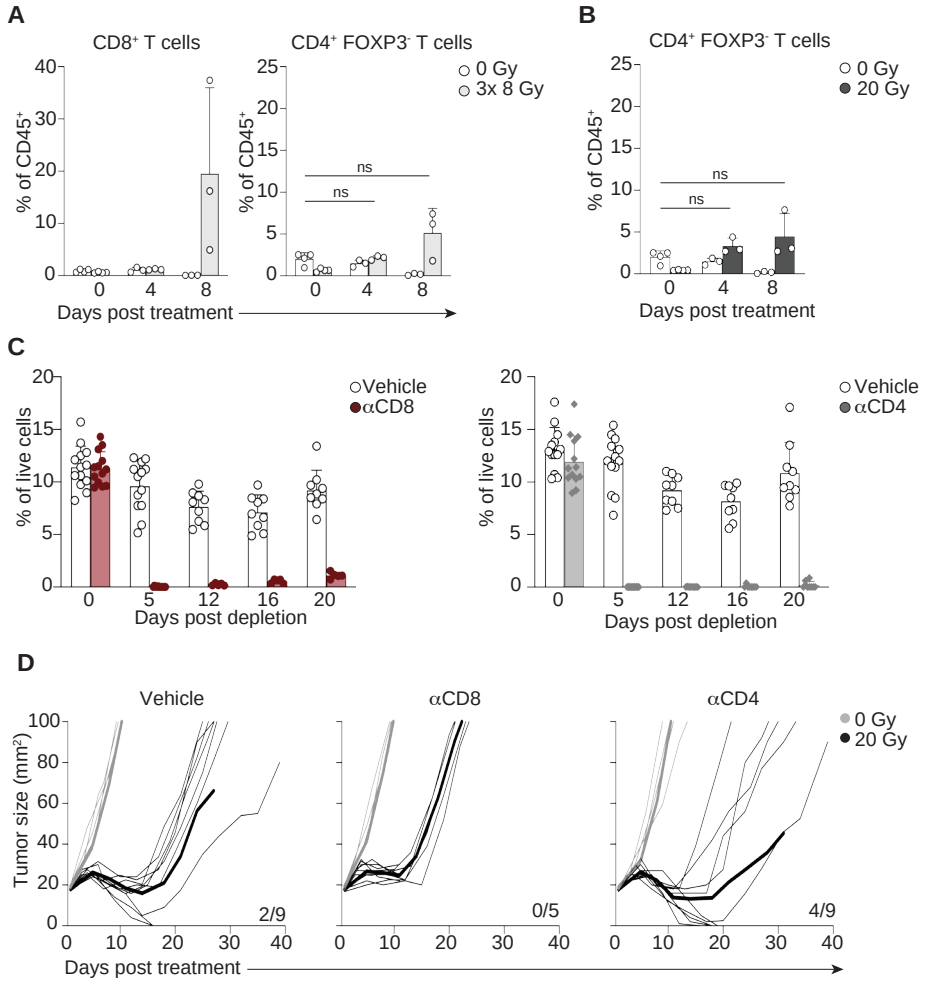

Supplemental Figure 2 – Related to Figure 2 (E - H)
(**A**,**B**) Monitoring by flow cytometry of the indicated immune cells over time in TC-1 tumors treated as control (0 Gy, n = 3-4/timepoint) or with either (**A**) 8 Gy over 3 days (3x 8 Gy, n=3-4/timepoint) or (**B**) a single dose of 20 Gy RT (n=3-4/timepoint). Error bars indicate SD. Kruskal-Wallis test with Dunn's post hoc analysis. (**C,D**) TC-1 tumor bearing mice were treated with 20 Gy RT (n=9/group) or control (0 Gy, n=4/group) at day 0 in combination with vehicle (PBS) or depleting mAbs against CD8 or CD4. (**C**) Frequency of CD8⁺ (left) or CD4⁺ Tconvs (right) among live cells in blood over time. The 0 Gy control group and 20 Gy groups are combined (Vehicle (PBS), n=13; αCD8, n=13; αCD4, n=13). (**D**) Individual tumor outgrowth curves belonging to Figure **2H**. Thick lines indicate group averages. Error bars indicate SD. ns; not significant. Data is from one experiment, representative of two experiments.

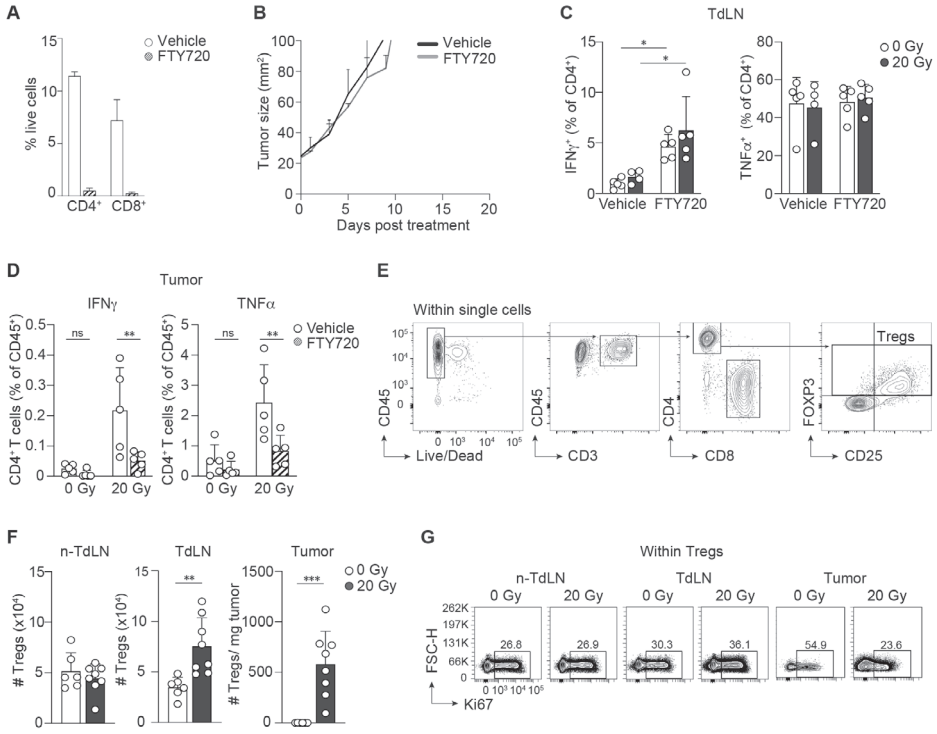

Supplemental Figure 3 – Related to Figure 3 (A – H).
(**A-D**) Data is from the same experiment described in Figure **3A-D**. TC-1 tumor bearing mice received 20 Gy RT (n=4-5/group) or 0 Gy (n=5) when tumor sizes reached ~20 mm^2 (day 0) in combination with FTY720 or vehicle (NaCl) by oral gavage, starting at day -1 and followed by days 3 and 5. At day 8, the TdLN and tumor were isolated and the $CD4^+$ T cell response was analyzed. (**A,B**) Frequency of $CD4^+$ and $CD8^+$ Tconvs among live cells in blood at day 5 (**A**) and average tumor outgrowth curves (**B**) in TC-1 tumor bearing mice treated with 0 Gy and FTY720 or vehicle. (**C,D**) Frequency of $IFN\gamma^+$ and $TNF\alpha^+$ cells within $CD4^+$ T cells in the TdLN (**C**) and in the tumor (**D**) of mice treated with 0 Gy or 20 Gy.(**E-G**) Monitoring of the ($FOXP3^+$ $CD25^+$) Treg response to 20 Gy RT (n=8) or 0 Gy (n=6) in TC-1 tumor bearing mice by flow cytometry at day 8 post treatment. (**E**) Representative gating strategy of Treg cells, based on $FOXP3^+$ and $CD25^+$ expression. (**F**) Absolute counts (#) of total Treg cells in the non-TdLN, TdLN and tumor. (**G**) Representative concatenated (0 Gy, n=6; 20 Gy, n=8) flow cytometry plots depicting $Ki67^+$ cells among Treg cells found in the non-TdLN, TdLN and tumor at day 8 post treatment. Numbers indicate the percentage of $Ki67^+$ cells. Data is from one experiment, representative of two experiments. Error bars indicate SD. *P < 0.05, **P < 0.01, *** P < 0.001, two-way Anova with Tukey's post hoc test in **C** and **D**, Mann-Whitney test in **F**. ns; not significant.

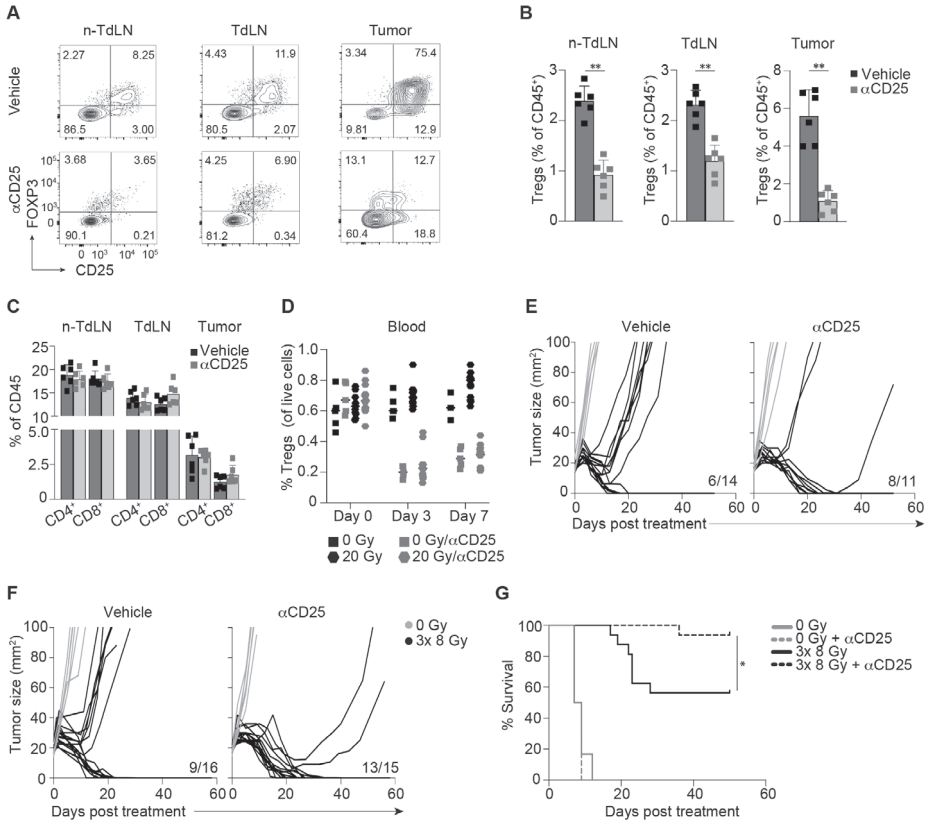

Supplemental Figure 4 - Related to Figure 3(I)

(**A-C**) TC-1 tumor bearing mice were treated i.p. with a depleting mAb against CD25 (n=6) or vehicle (PBS, n=6) when tumor size reached ~20 mm^2 (day 0). At day 4, the non-TdLN, TdLN and tumor were harvested and the Treg response was analyzed by flow cytometry. (**A**) Representative flow cytometry plots and (**B**) quantification depicting the frequency of total Tregs in the indicated tissues. (**C**) Proportion of $CD4^+$ and $CD8^+$ Tconvs among $CD45^+$ cells found in the indicated tissues following treatment. (**D**) Frequency of total Tregs among live cells measured in blood over time in the indicated treatment groups and (**E**) the individual tumor growth curves of the data described in Figure **3I.** (**F**) Individual tumor growth curves and (**G**) overall survival of TC-1 tumor bearing mice treated with 0 Gy (n=6) or 3x8 Gy (n =15-16) in combination with a depleting mAb against CD25 or vehicle (PBS) at day -1 and 5 post RT. Ratios indicate the number of mice that showed full recovery upon treatment. Data are from one experiment representative of two experiments. Error bars indicate SD. *P < 0.05, **P < 0.01, Mann-Whitney test in **B**, Mantel-Cox analysis in **G** and Kruskal-Wallis test with Dunn's post hoc test in **H**. ns; not significant.

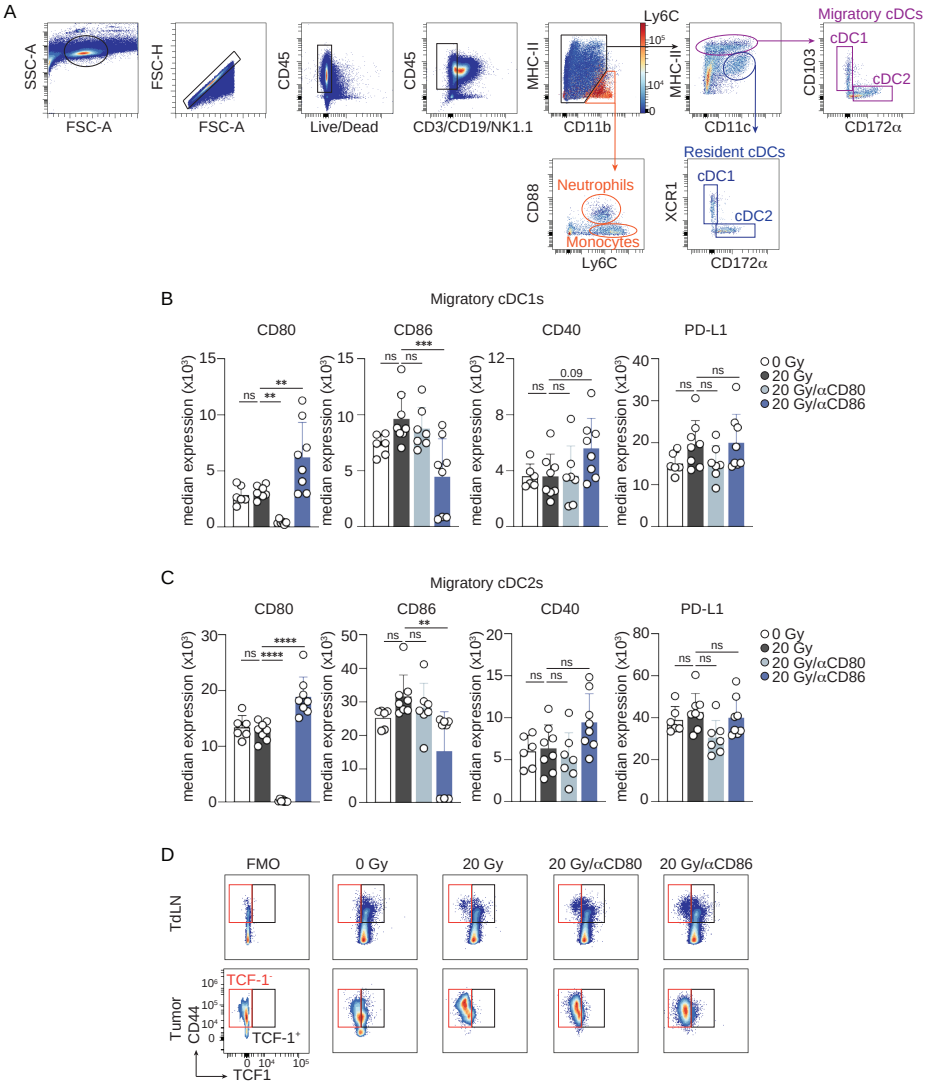

Supplemental Figure 5 – Related to Figure 6

(**A**) Representative gating strategy of cDC subsets in the TdLN of TC-1 tumor bearing mice. (**B**,**C**) Mice bearing 20 mm^2 TC-1 tumors received control treatment (0 Gy, n=6) or 20 Gy RT at day 0 in combination with either vehicle (PBS, n=8) or blocking mAb against CD80 (n=7) or CD86 (n=8) at day 0, 3 and 6. The cDC response was monitored by flow cytometry in the TdLN at day 8. (**B**,**C**) Median expression of the indicated markers found on (**B**) migratory cDC1s and (**C**) migratory cDC2s in the TdLN.(**D**) Representative gating strategy of the $CD44^+$ $TCF\text{-}1^-$ cells (orange) and $CD44^+$ $TCF\text{-}1^+$ cells (black) among $CD8^+$ T cells in the TdLN (upper row) and tumor (lower row) for the indicated treatment groups at day 8. FMO; fluorescence minus one. Data are from one experiment representative of two experiments. Error bars indicate SD. **P < 0.01, *** P < 0.001, **** P < 0.0001, ordinary one-way Anova with Dunnett's post hoc test in **C, D**. ns; not significant.

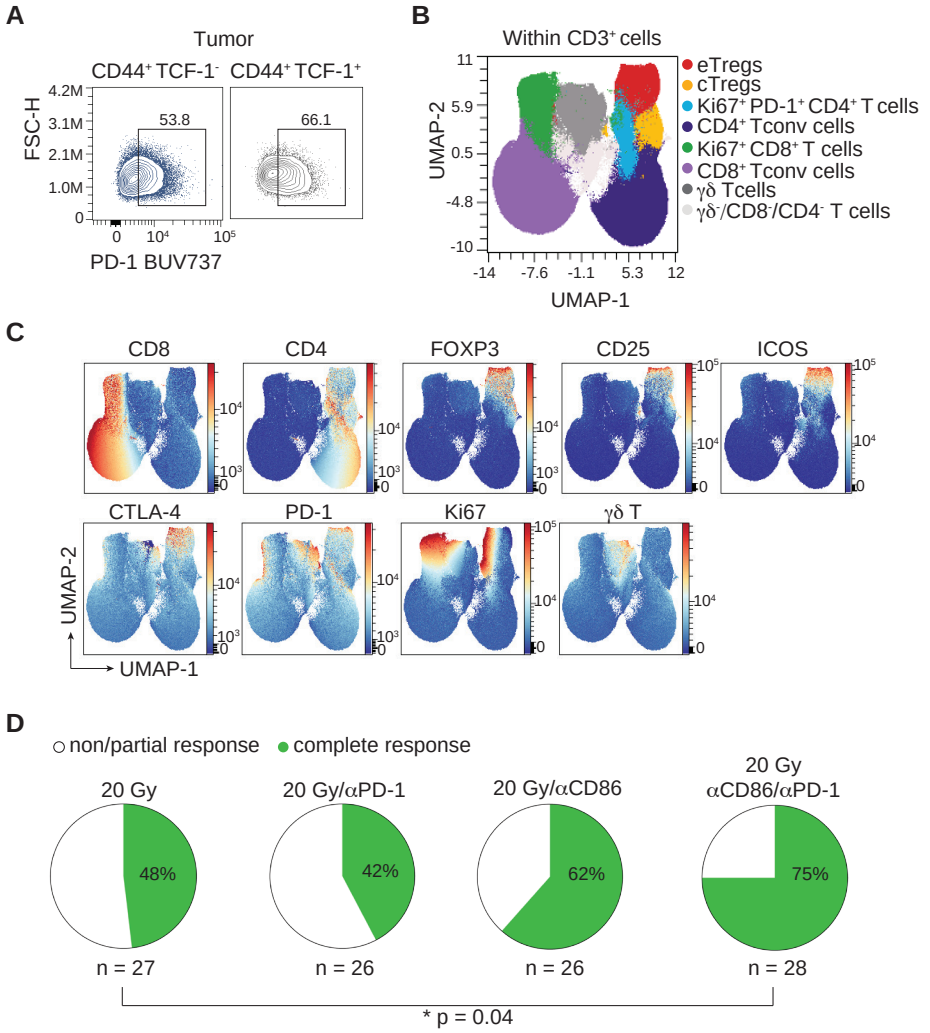

Supplemental Figure 6 – Related to Figure 7

(**A**) Mice bearing 20 mm^2 TC-1 tumors received control treatment (0 Gy, n=5) or 20 Gy RT at day 0 in combination with either vehicle (PBS, n=8) or blocking mAb against CD80 (n=11) or CD86 (n=11) at day 0, 3 and 6. The CD8$^+$ T cell response was monitored by flow cytometry in the tumor at day 8. Representative concatenated (n=11) contour plots are depicted for PD-1 expression on the indicated cell populations among CD8$^+$ T cells in mice treated with 20 Gy and CD86 blockade. Numbers indicate percentages. (**B-C**) Mice bearing TC-1 tumors received control treatment (0 Gy, n=4) or 20 Gy RT at day 0 in combination with either vehicle (PBS, n=8) or blocking mAb against PD-1 (n=11), CD86 (n=10) or a combination of both (n=10) at day 0, 3 and 6. The CD3$^+$ lymphocyte response was monitored by flow cytometry in the non-TdLN, TdLN and tumor at day 8. UMAP display of 2500 randomly selected CD3$^+$ cells per tissue found in non-TdLN, TdLN and tumors at day 8 of all treatment groups combined. FlowSOM guided clustering (**B**) identifying the CD3$^+$ cell populations and (**C**) representative heat map visualization of the markers that identify the CD3$^+$ (T-cell) subpopulations. (**D**) Pie chart depicting the proportion of TC-1 tumor-bearing mice with complete tumor clearance upon treatment with 20 Gy at day 0, in combination with either vehicle (PBS), or blocking mAb against PD-1, CD86 or both CD86 and PD-1 at day 0, 3 and 6. *P<0.05, Chi-square test.

Table 1: Antibodies & Reagents

Flow Cytometry Antibodies				
Antigen	*Fluorochrome*	*Clone*	*Vendor*	*Catalog #*
CD11c	BUV496	HL3	BD Biosciences	750483
CD11b	BV510	M1/70	BioLegend	101263
CD19	PerCP/Cy5.5	6D5	BioLegend	115534
CD25	BV421	7D4	BD Biosciences	564571
CD3	PerCP/Cy5.5	17A2	BD Biosciences	560527
CD3	BV785	17A2	Biolegend	100232
CD3	PE Cy7	145-2C11	eBiosciences	25-0031-81
CD4	BV711	GK1.5	BD Biosciences	563050
CD4	FITC	RM4-4	BioLegend	116003
CD4	BUV395	GK1.5	BD Biosciences	563790
CD40	PE Cy5	3/23	Biolegend	124617
CD43	PE Cy5	1B11	Biolegend	121216
CD44	BV785	IM7	Biolegend	103059
CD45	APC/Fire810	30-F11	BioLegend	103173
CD45	BUV395	30-F11	BD Biosciences	564279
CD45	BUV563	30-F11	BD Biosciences	612924
CD62L	APC/Cy7	MEL-14	BD Biosciences	560514
CD64	AF647	X54-5/7.1	BioLegend	139322
CD8	PerCP/Cy5.5	53-6.7	eBiosciences	45-0081-82
CD8	BUV805	53-6.7	BD Biosciences	612898
CD8	AF700	53-6.7	BioLegend	100730
CD80	PE/Dazzle 594	16-10A1	Biolegend	B271480
CD86	BV785	GL-1	Biolegend	B347725
CD88	BUV805	20/70	BD Biosciences	748611
CD103	BV711	M290	BD Biosciences	564320
CD172a	BUV395	P84	BD Biosciences	740282
CTLA-4	BV605	UC10-4B9	BioLegend	106323
CX3CR1	PerCP/Cy5.5	SA011F11	Biolegend	B318597
F4/80	BV421	BM8	BioLegend	123137
FOXP3	APC	FJK-16S	eBiosciences	25-5773-82
FOXP3	PE Cy5.5	FJK-16S	eBiosciences	35-5773-80
Granzyme B	PE	GB11	Sanquin	M2289
Helios	PE Cy7	22F6	BioLegend	137235
ICOS	PerCP/Cy5.5	C398.4A	BioLegend	313518
IFNy	eFluor450	XMG-1.2	eBiosciences	48-7311-82
IRF8	APC	V3GYWCH	eBisociences	17-9852-80
Ki67	AF700	SolA15	eBiosciences	56-5698-82
Ki67	eFluor506	SolA15	eBiosciences	69-5698-80
KLRG1	PE eF610	2F1	Thermo Fisher	4335245
Ly6C	Pacific Blue	HK1.4	BioLegend	128014
MHCII	APC-eFluor780	M5/114.15.2	eBiosciences	47-5321-80
NK1.1	PerCP/Cy5.5	PK136	BioLegend	108727
PD-1	BUV737	J43	eBiosciences	376-9985-80
PD-L1 (CD274)	BUV737	MIH5	BD Biosciences	741877
TCF-1	APC	C63D9	Cell Signaling Technology	37636S
TCRb	PE Cy7	H57-597	Biolegend	109222
TCRb	BUV563	H57-597	BD Biosciences	748406
TNFa	PE Cy7	MP6-XT22	BD Biosciences	561041
yd T cell	BV510	GL3	BioLegend	118131

Viability dyes		
LIVE/DEAD™ Fixable Near-IR Dead Cell Stain Kit	Thermo Fisher	L10119
Zombie UV™ Fixable Viability Kit	BioLegend	423107
Zombie Red™ Fixable Viability Kit	BioLegend	423109

In vivo antibodies & reagents				
Antigen	**Immunogen**	**Clone**	**Vendor**	**Catalog #**
CD25	IgG2a	M2A	Evitria	Gift from S. Quezada (under MTA)
CTLA-4	IgG2a fusion protein	UC10-4F10-11	BioXcell	BE0032
PD-1	Rat IgG2a	RMP1-14	BioXcell	BE0146
CD80	Rat IgG2a	1G10	BioXcell	BE0134
CD86	Rat IgG2a	GL-1	BioXcell	BE0025
CD8	Rat IgG2b	2.43	BioXcell	BE0061
CD4	Rat IgG2b	GK1.5	BioXcell	BE0003-1
FTY720			Cayman Chemical Company	10006292

Table 2: TCGA abbreviations

TCGA Abbreviation	Cancer Type
ACC	Adrenocortical carcinoma
BLCA	Bladder urothelial carcinoma
BRCA	Breast invasive carcinoma
CESC	Cervical squamous cell carcinoma and endocervical adenocarcinoma
CHOL	Cholangiocarcinoma
COAD	Colon adenocarcinoma
DLBC	Lymphoid Neoplasm Diffuse Large B-cell Lymphoma
ESCA	Esophageal carcinoma
GBM	Glioblastoma multiforme
HNSC	Head and Neck squamous cell carcinoma
KICH	Kidney Chromophobe
KIRC	Kidney renal clear cell carcinoma
KIRP	Kidney renal papillary cell carcinoma
LGG	Brain Lower Grade Glioma
LIHC	Liver hepatocellular carcinoma
LUAD	Lung adenocarcinoma
LUSC	Lung squamous cell carcinoma
MESO	Mesothelioma
OV	Ovarian serous cystadenocarcinoma
PAAD	Pancreatic adenocarcinoma
PCPG	Pheochromocytoma and Paraganglioma
PRAD	Prostate adenocarcinoma
READ	Rectum adenocarcinoma
SARC	Sarcoma
SKCM	Skin Cutaneous Melanoma
STAD	Stomach adenocarcinoma
TGCT	Testicular Germ Cell Tumors
THCA	Thyroid carcinoma
THYM	Thymoma
UCEC	Uterine Corpus Endometrial Carcinoma
UCS	Uterine Carcinosarcoma
UVM	Uveal Melanoma